CHALMERS
UNIVERSITY OF TECHNOLOGY

Measurement and Simulation of Cable Impedance Parameters in 600 V System

Master's thesis in Electric Power Engineering
in cooperation with Volvo GTT

AFRAAH FATHIMA BURHANUDDIN

HARESH VISWANATHAN

Department of Energy and Environment
CHALMERS UNIVERSITY OF TECHNOLOGY
Gothenburg, Sweden 2017

Master's thesis 2017:NN

Measurement and Simulation of Cable Impedance Parameters in 600 V System

Afraah Fathima Burhanuddin
Haresh Viswanathan

CHALMERS
UNIVERSITY OF TECHNOLOGY

Department of Electrical Engineering
Division of Electric Power Engineering
Chalmers University of Technology
Gothenburg, Sweden 2017

Measurement and Simulation of Cable Impedance Parameters in 600 V System
AFRAAH FATHIMA BURHANUDDIN
HARESH VISWANATHAN

Supervisor: Jörgen Kjellberg, Johan Björk-Svensson
Electromobility Department, Volvo GTT
Göteborg, Sweden

Examiner: Tarik Abdulahovic,
Chalmers University of Technology
Department of Electrical Engineering
Division of Electric Power Engineering
412 96 Gothenburg, Sweden.

Master's Thesis 2017:NN
Department of Electrical Engineering
Division of Electric Power Engineering
Chalmers University of Technology
SE-412 96 Gothenburg
Telephone +46 31 772 1000

Cover: A Volvo plug-in hybrid bus used for measurements.

Typeset in LaTeX
Printed by Chalmers Reproservice
Gothenburg, Sweden 2017

Measurement and Simulation of Cable Impedance Parameters in 600 V System
AFRAAH FATHIMA BURHANUDDIN
HARESH VISWANATHAN
Department of Electrical Engineering
Chalmers University of Technology

Abstract

This thesis presents measurement and simulation technique of cable impedance parameters in 600 V system. Coaxial and twinaxial cables are the two types of cables analyzed. The cables are modelled in finite element method (FEM) software using the concept of transverse electric magnetic (TEM) waves. The impedance parameters are measured in a laboratory with a vector network analyzer (VNA) using short circuit and open circuit method. A comparison and analysis of results is made between the simulation and laboratory measurements. The effect on the impedance parameters due to a solid or braided shield in a cable are discussed. Also, a study is conducted to understand the behaviour of cable impedance for placements and at different heights from chassis/copper frame. Different types of shield groundings are adopted in the measurement setup to understand its main purpose. Furthermore, measurements on the cables of a hybrid bus are also performed and compared with the simulation and laboratory measurement results.

Keywords: Finite Element Method (FEM), Vector Network Analyzer (VNA), Coaxial, Twinaxial, Grounding, Shield, Coupling

Acknowledgements

First of all, We would like to express our gratitude to Jörgen Kjellberg and Johan Björk- Svensson for the opportunity to do our Master's thesis at the electromobility department and for providing continuous support at Volvo GTT. We would also like to thank Per Widek for sharing his knowledge and experience about the project. Secondly, we would like to thank our examiner Tarik Abdulahovic, professor at Chalmers University of Technology for the technical discussions, guidance and thoughtful ideas for the thesis work which has led us forward.

Afraah Burhanuddin & Haresh Viswanathan, Gothenburg, August 2017

Contents

List of Figures

List of Tables

1
Introduction

1.1 Problem Background

With the current scenario where the non-renewable resources are draining at an alarming rate and with the development in the electric/hybrid vehicle sector, it is the perfect time to augment their research, development and production. Electric/hybrid vehicles are a significant step towards reduction in carbon emissions that are emitted into the atmosphere [4].

Vehicles that use more than one source of energy for propulsion are termed as an electric hybrid vehicle. The electric hybrid system combines a conventional internal combustion engine (ICE) with an electric propulsion system (EPS). The main components of an EPS consists of electrical storage system (ESS), power electronics (PE), electric machine (I-SAM), electric motor drive (EMD) which controls the electric machine, and electrified auxiliaries. The electrified auxiliaries consists of air compressor, heat ventilation and air conditioning (HVAC), DC/DC converter and power steering. A fully electric driveline replaces the ICE with a larger battery pack for propulsion [4, 7]. Electrification of cars and heavy vehicles differ in a way that the latter requires higher power for propulsion than the former.

In general, electrification of ICE vehicles has led to incorporation of several electrical and power electronic components which vary in frequencies and impose a greater challenge on the manufacturers to reduce the electromagnetic fields. The high voltage cables and connectors enable power transfer from one component to other throughout the EPS. Electromagnetic field emissions emitted from different components in EPS are radiated through these high voltage cables. High voltage and high electrical currents generate higher electric and magnetic fields which can cause interference with other electrical equipments. These emissions can couple with nearby components which can cause malfunctioning and environmental problems [4, 6, 5]. Also, cable routing and layouts affect the overall system performance. Hence it is necessary to study these effects on impedance of the cable and minimize electromagnetic fields to meet the EMC safety standards.

Volvo group is working on measurement methods and simulation strategies to calculate the impedance of different components in the EPS to minimize this electromagnetic interference (EMI) thereby reducing the current/voltage ripple across DC link capacitor in the inverter bridge. In this thesis, the focus is narrowed down to de-

velop a suitable measurement method to calculate the impedance parameters of high voltage cables and it is compared with finite element method (FEM) simulations for different hybrid/electric vehicles.

1.2 Previous Work

The previous work was carried out by two students from Lund University. The aim of their thesis was to study the current ripple across DC link capacitor of the EMD inverter in order to analyze the influence of ripple by EPS components and also increase their lifetime. The study was carried out by a system level decomposition of EPS of hybrid and electric bus. A spice model with sub-systems of the various components were modelled and simulated. Component values were obtained from the Volvo employees, suppliers and measurements. Later, verification tests on hybrid bus were done to validate simulations results for comparison. This study showed that spice model was inconsistent for battery, DC cables and filters [8].

1.3 Purpose of this work

The spice model of the EPS was found to be sensitive to alterations with cable parameters and so it is necessary to investigate the ripples that propogate through the cables at various frequencies, installation and placement. Even though the cable parameters were provided by the supplier, these values need to be checked with FEM simulations and laboratory measurements. Also, the results of this thesis are an improvement to the existing spice model so that it can be accurate enough to evaluate the DC link ripple.

1.3.1 Scope

In this thesis, test cables with braided shield were used for measurement but in FEM analysis, cables with solid shield were simulated. A solid shield will only be considered for the FEM simulations, due to the difficulty and time consumed in designing a braided shield. A perfectly shielded cable has the following properties mentioned below.

1. The shield completely encloses the conductor. In other words the center conductor does not exceed beyond the shield.
2. The shield is completely solid - meaning there are no holes as in case of braided shield
3. The shield is not terminated by any impedance.

1.3.2 Sustainability aspects

Fossil fuel powered vehicles have always dominated automobile industry even though electric vehicles have existed since 1900s [7]. Environmental concerns such as pollution, global warming, limited resource availability has lead to renewed interests in alternative bio-fuels and electric vehicles. Electric vehicles are seen as a stepping-stone

towards a sustainable future. Hybrid and plug in electric vehicles are a response from automotive manufacturers to reduce carbon dioxide emissions. Off-course, these vehicles can lower the carbon emission from the exhaust of their tail pipe, but, whether the overall implementation will help in reduction of the carbon emission is a subject to question. Electric vehicles can be considered sustainable only if the electricity to drive them is generated from renewable energies such as wind, solar, hydroelectric energy. If electric vehicles were to be powered by conventional energy sources, this would aggravate the environmental issues. Electric vehicles also reduce noise pollution on motorways where houses are constructed near to them [4, 9].

Automotive manufacturers have increased their dependence on variety of metals that are used in different electric components in electric vehicles. These vehicles have additional components such as; battery, electric machine, power electronic converters, alternators and high voltage cables. The components are connected with long and thick copper cables. Dangerous elements such as Lithium, Nickel and Cobalt used in battery are obtained from mines and this can have an impact on environment and human health. Also, electric machines use rare earth metals such as neodymium, dysprosium [4]. These metals need to be extracted in large quantities so as to promote mass adoption of electric vehicles. It becomes necessary to question if these metals are available in large quantities to suffice global level EV production. Earth has limited minerals and resources and are bound to become scarce at a finite time. This would result in metal scarcity which can lead to hindrance in technology development. One solution to this would be to use alternate energy storage systems that do not use chemicals in their construction.

Replacing ICE vehicles with electrified vehicles is a challenging aspect. An overarching question to ask is if electric vehicles are safer without an IC engine. People are already aware about the risks involved in an ICE vehicle but the risks associated with electric vehicles are not known to most people. In electric vehicles, there could be a risk associated with having a large battery on board that can become dangerous during an event of accident. This type of safety issue can develop a negative impact among people for adoption of electromobility. A solution to this could be to use additives in the battery production that can buffer or minimize the risk associated with the battery. Also, EVs emit electromagnetic fields which can be harmful to human beings. These magnetic fields need to be well within the limiting values so that one can feel safe [4].

1.3.3 Ethical Codes

Some of the ethical codes that were follwed througout this thesis were:

- It is important to state claims/assumptions made in the simulations and measurements of the cable impedance. In a vehicle, there is usually a web of cables and it is impossible to measure accurate mutual impedance between the cables.

- As mentioned in the background, hybrid vehicles the electric and power elec-

tronic equipments generate electromagnetic fields; It is necessary that adopters of hybrid vehicles are aware of the risks involved with magnetic fields and these should be well within the engineering standards for human health safety.

- As we are students from a university who are constantly trying to learn as much as we can from electric power field, we value assistance given by our supervisors and colleagues as they have more experience and knowledge than us. Further it also necessary to check if information/opinion given by them is correct in case they do not have a clear picture about the objective of the thesis.

2

Theory

2.1 Test Cables

In this work two types of test cables have been examined. The first type of cable is a coaxial cable (shielded conductor) with a cross sectional area of 50 mm^2 and the second type of cable is a twinaxial shielded cable (two conductors with a common shield) of cross sectional area 2x4 mm^2.
The test cables are manufactured by Huber and Suhner AB. The manufacturer, claims that these cables are excellent to low pressure and high pressure, temperature, weather resistant and are suitable for automotive applications. The insulation and sheath material used is of RADOX which has excellent dielectric properties [12].

2.1.1 Co-axial cable

In coaxial cable, the conductor core comprises of bunches of bare copper strands. The conductor is surrounded by the first RADOX insulation layer which is referred to as the dielectric insulation. It prevents the shield and conductor coming in contact with each other. Next is the tin plated copper braid shield (also known as EMC screen) which confines the electromagnetic waves radiating from the conductor and precludes external electromagnetic waves (from surrounding components) from getting coupled to the conductor. It also provides a return path for the current flowing through the conductor and therefore. Since the copper conductor cross sectional area is smaller than the tin plated copper braid shield, a coaxial cable is also called as unbalanced cable [13]. The outermost layer of coaxial cable is the RADOX elastomer sheath which protects the conductor from moisture, abrasion and provides a close fitting cover for the inner layers.
A side view and cross sectional view of the 50 mm^2 cable is indicated in Figure 2.1. 'a', 'b', 'c', 'd' is the radius of conductor, dielectric insulation, EMC screen and sheath respectively.

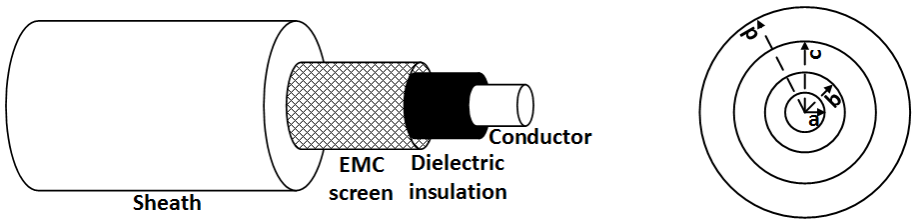

Figure 2.1: Coaxial cable side view (left) and cross sectional view (right)

2.1.2 Twinaxial Cable

The twinaxial cable comprises of two conductors composed of tin plated copper strands. Each conductor has a cross sectional area of 4 mm^2 and is surrounded by a RADOX insulation. One conductor provides path for incoming signal while the other conductor provides the return path for the same signal. Since the diameter of the conductors that carry incoming and return signal is the same, a twinaxial cable can also be known as a balanced cable [13]. The two conductors are enclosed together by a common shield which is also made of braided tin plated copper. Unlike the shield in coaxial cable, the shield in twinaxial cable does not carry any signal; its purpose is to reduce the external and internal electromagnetic radiations. In FEM model, this cable is assumed to have a elliptical geometry as indicated in the Figure 2.2.

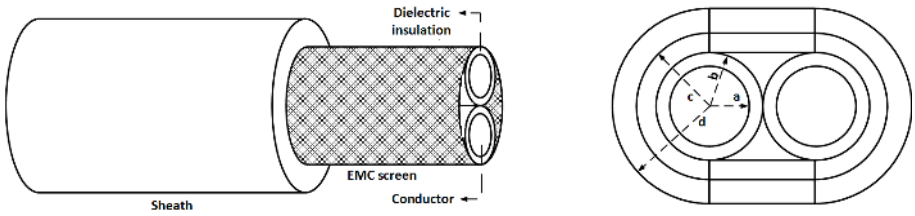

Figure 2.2: Twinaxial cable side view (left) and cross sectional view (right)

2.1.3 Difference between braided shield and solid shield

As mentioned in scope, the real test cables have a braided shield while in FEM model a solid shield was used. The differences one would expect when using a different type of shield need to be addressed.
Most cables have a braided shield instead of solid shield; this is because by using a braided shield, the cable becomes flexible, durable and has a long life. This comes with a trade-off; a braided shield can provide only a effective shielding of 60 to 98% unlike the high efficient shielding of a solid shield [1, 15]. This is due to the apertures or holes on the braid that can not enclose all of the electromagnetic waves formed when a signal flows through the conductor i.e. there is a leakage of these waves through these apertures.
Due to this leakage, the total inductance of the coaxial cable with a braided shield; which includes the self inductance of the conductor and mutual inductance is higher when compared with the total inductance of a coaxial cable with a solid shield. In order to prevent leakage of electromagnetic waves, multiple braided shields can be used. This increases the costs of cables and reduces their flexibility [1, 15].

2.2 Basics of electromagnetic theory

An electrical cable is a conductor with an overlying outer insulation with an optional metallic shielding which carries electric currents from source to the load. As length of a cable increases, it can be depicted as a transmission line (TL). In transmission line theory, there are three types of waves that can propagate down a TL ie.

transverse electric (TE), transverse magnetic (TM) and transverse electromagnetic waves (TEM). TEM waves can propogate only in multi-conductor TLs such as coaxial cable, two wire lines, while TE and TM can exist only in single conductor TL. In a TEM wave, electric and magnetic fields are transverse to each other along the direction of propagation [3, 10].

2.2.1 Telegrapher's equation

Cables are usually the longest parts in the EPS and are a major source to pick up or radiate noise in electromagnetic coupling. In this work, the loss parameters of a shielded coaxial cable and twinaxial cable will be discussed and analyzed. Since the length of the cable is small compared to its wavelength, the electromagnetic coupling between the cables are considered as lumped instead of distributed parameters [1]. If the testing frequency is high and propagation effects are not negligible, then distributed parameter modelling has to be considered [2].

Generally, in a two conductor transmission line, the currents and voltages vary in time and distance along its length as seen from Figure 2.3. This is due to the inductance and capacitance between the lines. The equations governing the change in voltage v(z,t) and current i(z,t) in time and distance is called telegraphers equations. From the figure, it can be noticed that there is conduction current flowing in the conductor and shield of the coaxial cable, and displacement currents between the two conductors. Each of these currents contribute to transmission line impedances.

1. Conduction current impedance
   - Resistance R, due to losses in the conductors and shield.
   - Inductance L, due to currents and magnetic flux linking the conductors.
2. Displacement current impedance
   - Conductance G, due to losses in dielectric between the conductors.
   - Capacitance C, due to time varying electric field between the conductors.

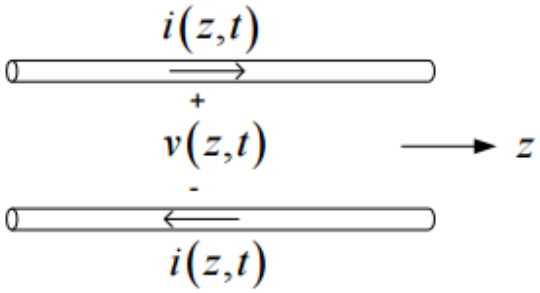

Figure 2.3: Voltage and current along the transmission line

A general transmission line model for obtaining telegrapher's equations is shown in the Figure 2.4. Applying Kirchoff's voltage and current laws in Figure 2.4, gives

$$v(z,t) = R\Delta z \cdot i(z+\Delta z,t) + L\Delta z \frac{\partial i(z+\Delta z,t)}{\partial t} + v(z+\Delta z,t) \qquad (2.1)$$

$$i(z,t) = G\Delta z \cdot v(z,t) + C\Delta z \frac{\partial v(z,t)}{\partial t} + i(z+\Delta z,t) \tag{2.2}$$

Rearranging and dividing the equations by Δz gives (2.3) and (2.4).

$$\frac{v(z,t) - v(z+\Delta z,t)}{\Delta z} = R\Delta z \cdot i(z+\Delta z,t) + L\Delta z \frac{\partial i(z+\Delta z,t)}{\partial t} \tag{2.3}$$

$$\frac{(z,t) - i(z+\Delta z,t)}{\Delta z} = G\Delta z \cdot v(z,t) + C\Delta z \frac{\partial v(z,t)}{\partial t} \tag{2.4}$$

As $\Delta z \to 0$ the equations becomes

$$\frac{\partial v(z,t)}{\partial z} = -R \cdot i - L\frac{\partial i(z,t)}{\partial t} \tag{2.5}$$

$$\frac{\partial i(z,t)}{\partial z} = -G \cdot v - C\frac{\partial v(z,t)}{\partial t} \tag{2.6}$$

Eq. (2.5) and (2.6) are called as transmission line equations or Telegrapher's equations.

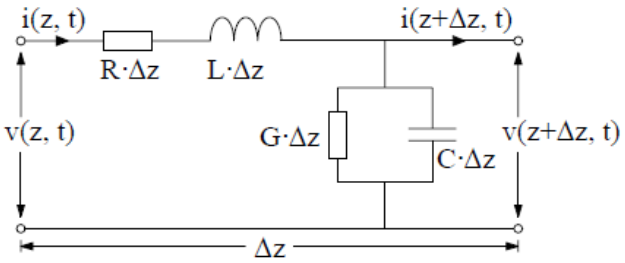

Figure 2.4: Voltage and current along the transmission line

2.3 Coupling between coaxial cables

There are three couplings considered depending on placement of the cable (near field or far field). The first is electric or capacitive coupling which results from interaction of electric fields between the two cables. Next is inductive or magnetic coupling which results from interaction of magnetic fields from the two cables. Finally, it is the electromagnetic coupling or radiation which results from interaction of both electric and magnetic fields [1]. Since the distance between the two cables are not large, it is considered as near field and hence the electric and magnetic fields are analyzed separately.

2.3.1 Effect of Shield on Capacitive Coupling

For modelling of cables in FEM, a perfectly shielded cable is assumed as mentioned in scope. In practical cases, a cable has a braided shield in which the center conductors may exceed beyond the shield; this gives rise to additional coupling parameters

which affects the impedance of the system. The physical representation of two shielded conductor in practical case is shown in Figure 2.5. In this Figure, C_{12} is the capacitance between conductor 1 and 2, C_{1S} and C_{2S} are the capacitances between the shield and conductor of individual cables, C_{1G} and C_{2G} are the capacitances of conductors 1 and 2 w.r.t ground and R is the resistance to ground. In most cases the resistance offered is very small. Therefore if,

$$R << \frac{1}{j\omega(C_{12} + C_{1G} + C_{1S} + C_{2G} + C_{2S} + 2C_{SG})} \tag{2.7}$$

then the noise voltage V_N picked up by conductor 2 due to voltage V_1 given by (2.8)

$$V_N = j\omega R C_{12} V_1 \tag{2.8}$$

It can be seen from (2.8) that the noise voltage is directly related to ground resistance and capacitive coupling. Hence these two parameters have to be kept as low as possible to reduce noise voltage when it is not possible to change any other parameters in (2.8).

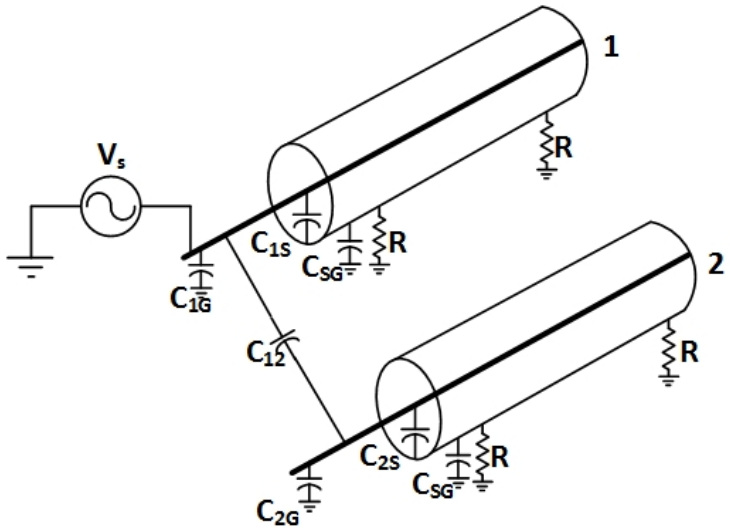

Figure 2.5: Physical representation of capacitive coupling in practical cases

2.3.2 Magnetic Coupling

When current flows through a circuit, it induces a flux in nearby circuit. This is know as mutual inductance. The voltage V_N induced in closed loop of area $\bar{A}$ and magnetic flux density $\bar{B}$ is given by Faraday's law (2.9).

$$V_N = -\frac{d}{dt}\int_A B.dA \tag{2.9}$$

where $\bar{A}$ and $\bar{B}$ are vectors. For stationary closed loop and sinusoidally time varying flux density, V_N is given by (2.10)

$$V_N = j\omega BAcos\theta \tag{2.10}$$

where θ is the angle between B and A. Since $BAcos\theta$ represents the flux linking the neighbouring circuit, the induced voltage V_N is given by (2.11)

$$V_N = j\omega M I_1 = M\frac{di_1}{dt} \tag{2.11}$$

where M is the mutual inductance and I_1 is the current flowing in source circuit. The physical representation of magnetic coupling between two shielded conductors in a practical case is shown in Figure 2.6

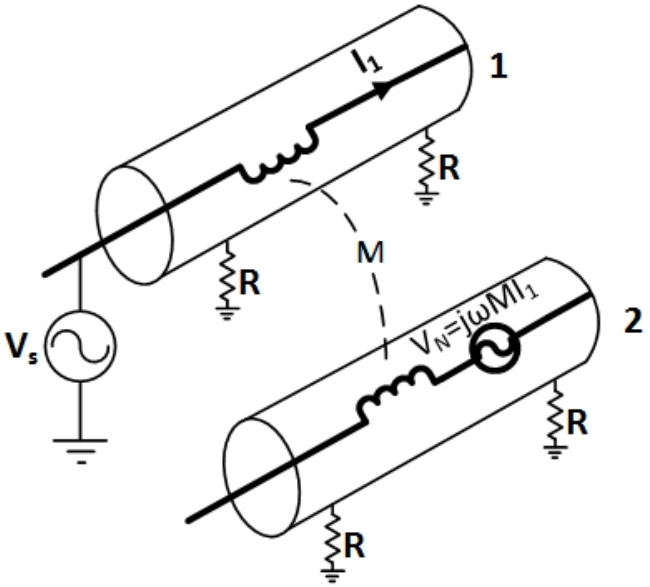

Figure 2.6: Physical representation of magnetic coupling in practical cases

2.3.2.1 Effect of Shield on Magnetic Coupling

In FEM simulations, it is assumed that the shield carries a current equal and opposite to the current in the conductor. The shield current generates an opposite external magnetic field of equal intensity to cancel out the fields generated by the conductor. The current flowing in the shield is given from Figure 2.7.
Applying mesh analysis in the Figure 2.7,

$$0 = -I_s(j\omega L_S + R_S) + j\omega M I_1 + I_G Z_G \tag{2.12}$$

where R_s is the resistance of the shield, L_s is the inductance of shield, M is mutual inductance between shield and conductor and I_1 is the current in the conductor. Equating for shield current from (2.12),

$$I_s = I_1\left(\frac{j\omega M}{j\omega L_s + R_s + Z_G} + \frac{Z_G}{j\omega L_s + R_s + Z_G}\right) \tag{2.13}$$

Since the mutual inductance between the shield and conductor is equal to self inductance of shield [1], (2.13) becomes

$$I_s = I_1\left(\frac{j\omega}{j\omega + \frac{R_s+Z_G}{L_s}} + \frac{Z_G/L_s}{j\omega + \frac{R_s+Z_G}{L_s}}\right) = I_1\left(\frac{j\omega}{j\omega + \omega_c} + \frac{Z_G/L_s}{j\omega + \omega_c}\right) \tag{2.14}$$

From (2.14) it can be seen that at frequencies higher than cut-off frequency of the shield (ω_c), the shield current approaches the conductor current. Hence all the current returns through the shield instead of flowing through the ground. At lower frequencies, a larger portion of the current flows through the ground thus reducing the shielding effectiveness of the cable.

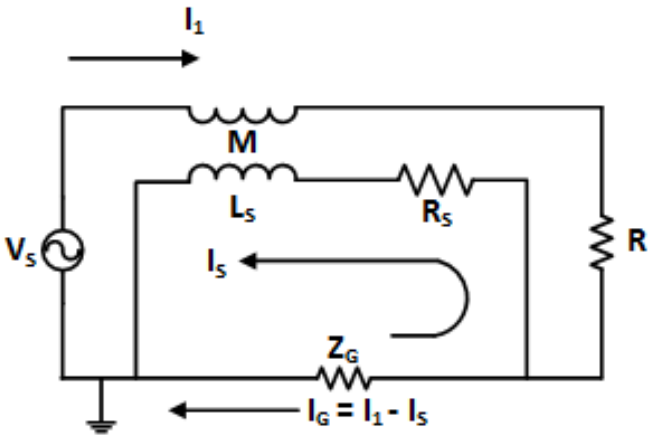

Figure 2.7: Effect of Shield on Magnetic Coupling

2.3.2.2 Crosstalk

Crosstalk is defined as an interference to a signal path from other signals within its close proximity. The electromagnetic interference between the cable can be either inductive coupling or capacitive coupling. For electrically short cables, the crosstalk can be modelled using lumped circuit analysis as shown in Figure 2.8. The signal is applied to one of the conductors and the coupling parameters are measured in the other conductor. Depending on the value of load R_L the coupling can be either inductive or capacitive. A small value of load represents a short circuit and gives inductive coupling between the conductors. A large value of load represents an open circuit and gives capacitive coupling between the conductors.

The coupling parameters measured at the same end as that of the input signal V_s is termed as near end crosstalk (NEXT). The coupling paramters measured on the other end of V_s is termed as far end crosstalk (FEXT). R_{NE} and R_{FE} represents near end and far end resistances. These value are kept the same as the load depending on the type of coupling to be measured [11]. The coupling parameters are obtained from solving (2.15) and (2.16).

$$\frac{V_{NE}}{V_s} = \underbrace{\frac{R_{NE}}{R_{NE}+R_{FE}} j\omega L_m \frac{1}{R_s+R_L}}_{InductiveCoupling} + \underbrace{\frac{R_{NE}R_{FE}}{R_{NE}+R_{FE}} j\omega C_m \frac{R_L}{R_s+R_L}}_{CapacitiveCoupling} \tag{2.15}$$

where R_s is the resistance of the source which is 50 Ω, L_m is inductive coupling and C_m is capacitive coupling

$$\frac{V_{FE}}{V_s} = \underbrace{-\frac{R_{FE}}{R_{NE}+R_{FE}} j\omega L_m \frac{1}{R_s+R_L}}_{InductiveCoupling} + \underbrace{\frac{R_{NE}R_{FE}}{R_{NE}+R_{FE}} j\omega C_m \frac{R_L}{R_s+R_L}}_{CapacitiveCoupling} \tag{2.16}$$

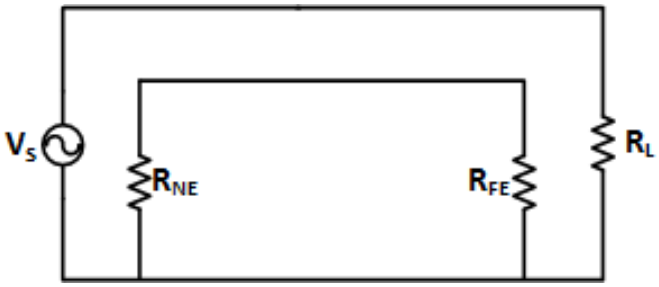

Figure 2.8: Crosstalk in cables

2.4 Grounding of cable shields

2.4.1 Low frequency grounding

The main purpose of grounding the shields at lower frequencies is to protect against electric field coupling. In case of coaxial cables, the shield current generates a noise voltage that cancels the fields generated from the conductor. At frequencies lower than shield cut off frequency, it is recommended to ground only at one end to avoid the ground loop current and additional losses. EMC standards recommend to ground at the source end since it provides reference for the input signal. With the source floating, it is recommended to ground at the load side. Grounding at source end will cause the entire current to flow through the shield since the shield is used as a return path [1].
In case of multiconductor cables where the shield is not used as a return path, it is recommended to ground only at one end. If it is grounded at more than one end then a noise voltage is generated due to difference in potential between the ends which disrupts the fields in the conductors.

2.4.2 High frequency grounding

At frequencies above five times the shield cut off frequency or when the cable length exceeds one-quarter of the wavelength, it is recommended to ground at both the ends for a coaxial cable. This is because at higher frequencies, the shield acts as an antenna at the ungrounded end and can obtain enough field strength to couple to the ground. At frequencies above 100 kHz it is necessary to ground both the ends in coaxial and twinaxial cable because the stray capacitance couples to the ground loop [1].

3

Case set-up

3.1 FEM Modelling of coaxial and twinaxial cables

Coaxial and twinaxial cables are modelled in FEM using waveguiding systems. Waveguides are used to transfer electromagnetic energy from one point to another point in space. Since in cables, the electromagnetic energy is transferred from a positively charged conductor to a negatively charged conductor, the concept of transverse electric magnetic (TEM) can be utilized in modelling a multi-conductor cable [3].

3.1.1 Longitudinal-Transverse Decompositions

The Maxwell's equations are solved along the propagating direction in waveguiding systems [3]. Hence, the electric and magnetic fields are given the form (3.1),

$$\begin{aligned} E(x,y,z,t) &= E(x,y)e^{j\omega t - j\beta z} \\ H(x,y,z,t) &= H(x,y)e^{j\omega t - j\beta z} \end{aligned} \tag{3.1}$$

where β is the propagation wave number. Maxwell's equations from (3.1) are decomposed into longitudinal component along z-direction and transverse components along x, y directions.

$$E(x,y) = \underbrace{\hat{x}E_x(x,y) + \hat{y}E_y(x,y)}_{transverse} + \underbrace{\hat{z}E_z(x,y)}_{longitudinal} = E_T(x,y) + \hat{z}E_z(x,y) \tag{3.2}$$

Decomposing the gradient operator gives (3.3)

$$\nabla = \underbrace{\hat{x}\partial_x + \hat{y}\partial_y}_{transverse} + \hat{z}\partial_z = \nabla_T + \hat{z}\partial_z = \nabla_T - j\beta\hat{z} \tag{3.3}$$

Since the assumed propagation direction is along z, from (3.3) $\partial_z = -j\beta$. Substituting these expressions in source free Maxwell's equations,

$$\left.\begin{aligned} \nabla \times E &= -j\omega\mu H \\ \nabla \times H &= j\omega\epsilon E \\ \nabla \cdot E &= 0 \\ \nabla \cdot H &= 0 \end{aligned}\right\} \implies \left\{\begin{aligned} (\nabla_T - j\beta\hat{z}) \times (E_T + \hat{z}E_z) &= -j\omega\mu(H_T + \hat{z}H_z) \\ (\nabla_T - j\beta\hat{z}) \times (H_T + \hat{z}H_z) &= -j\omega\mu(E_T + \hat{z}E_z) \\ (\nabla_T - j\beta\hat{z}) \cdot (E_T + \hat{z}E_z) &= 0 \\ (\nabla_T - j\beta\hat{z}) \cdot (H_T + \hat{z}H_z) &= 0 \end{aligned}\right.$$

where μ and ϵ are the permittivity's of the medium. Equating the longitudinal and transverse parts of source free Maxwell's equations, an equivalent set of equations is obtained in (3.4)

$$\begin{aligned} \nabla_T \times \hat{z} - j\beta\hat{z} \times E_T &= -j\omega\mu H_T \\ \nabla_T \times \hat{z} - j\beta\hat{z} \times H_T &= -j\omega\epsilon E_T \\ \nabla_T \times E_T + j\omega\mu\hat{z}H_z &= 0 \\ \nabla_T \times H_T - j\omega\epsilon\hat{z}E_z &= 0 \\ \nabla_T \cdot E_T - j\beta E_z &= 0 \\ \nabla_T \cdot H_T - j\beta H_z &= 0 \end{aligned} \tag{3.4}$$

In case on TEM, the terms $E_z = H_z = 0$ defining the electric and magnetic fields are transverse with each other and is independent of the propagation direction.

3.1.2 Transmitted Power

The inductance (L) and capacitance (C) parameters are obtained from transmitted power (P_z) expressions in TEM. The transmitted power is obtained by integrating along z-direction of the Poynting vector over the cross section of the geometry. For TEM mode $P_z = |E_T|^2/2\eta$, where η is the medium impedance $\sqrt{\frac{\mu}{\epsilon}}$ [3].

$$P_T = \frac{1}{2\eta}\iint_S |E_T|^2 dxdy = \frac{1}{2\eta}\iint_S |\nabla_T\varphi|^2 dxdy = \frac{1}{2}Z|I|^2 \tag{3.5}$$

Since TEM is solved for electric and magnetic fields, the electromagnetic energy distribution is given by time averaged electric and magnetic field densities per unit length as shown in (3.6) and (3.7)

$$W_e = \frac{1}{4}\epsilon\iint_S |E_T|^2 dxdy = \frac{1}{4}C|V|^2 \tag{3.6}$$

$$W_e = \frac{1}{4}\epsilon\iint_S |H_T|^2 dxdy = \frac{1}{4}L|I|^2 \tag{3.7}$$

3.1.3 Resistance and Conductance

The resistance of the cables are obtained from conductor ohmic losses. The coaxial cable has currents incoming at the conductor and returning through the shield while the twinaxial cable has a separate return conductor. Assuming the conductivities of the dielectric is zero, the conductor power loss per unit length for coaxial and twinaxial is given by (3.8)

$$P_{loss} = \frac{1}{2}R\oint_{conductor} |H_T|^2 dl + \frac{1}{2}R\oint_{return} |H_T|^2 dl \tag{3.8}$$

Since $|H_T|$ is related to current I, the conductor ohmic loss is given by 3.9,

$$P_{loss} = \frac{1}{2}R|I|^2 \tag{3.9}$$

In this case a lossy dielectric medium is assumed which means the dielectric between the conductor and shield is slightly conducting. The shunt conductance per unit length can be written as shown in (3.10)

$$G = \frac{\omega\epsilon''}{\epsilon}C \tag{3.10}$$

where ϵ'' is loss parameter of dielectric.

3.1.4 Analytical representation of coaxial cables

Since there are well defined analytical expressions for coaxial cables at different frequencies, they were used to validate the approach for FEM simulations. The loss parameter expressions for a coaxial cable with conductor radius 'a', dielectric radius 'b' and EMC screen radius 'c' shown in Figure 2.1 at various frequency ranges are obtained from [10].

3.1.4.1 High frequencies (HF)

The resistance (Ω/m) per unit length is given by (3.11)

$$\begin{aligned} R &= \frac{R_s}{2\pi}(\frac{1}{a}+\frac{1}{b}) \\ R_s &= \frac{1}{\sigma_c\delta} \quad and \\ \delta &= \sqrt{\frac{2}{\mu_r\mu_0\omega\sigma_c}} \end{aligned} \tag{3.11}$$

where σ_c is conductivity of copper in [S/m], δ is the skin effect in [m], μ_0 is the permeability of free space and μ_r is the relative permeability of the material.

The inductance (H/m) per unit length is given by (3.12)

$$L = \frac{\mu_0\mu_r}{2\pi}ln(\frac{b}{a}) + \frac{\mu_0\mu_r\delta}{4\pi}(\frac{1}{a}+\frac{1}{b}) \qquad (H/m) \tag{3.12}$$

The capacitance (F/m) per unit length is given by (3.13)

$$C = \frac{2\pi\epsilon_0\epsilon'}{ln(\frac{b}{a})} \qquad (F/m) \tag{3.13}$$

where ϵ_0 is the permittivity of free space and ϵ' is the real term of relative permittivity of the dielectric.

The conductance per unit length is given by (3.14)

$$G = \frac{2\pi\omega\epsilon_0\epsilon''}{ln(\frac{b}{a})} \qquad (S/m) \tag{3.14}$$

where ϵ'' is the lossy term of the dielectric.

The characteristic impedance of the cable is given by (3.15)

$$Z = \frac{Z_{0,const}}{2\pi}\sqrt{\frac{\mu_r}{\epsilon_r}}ln\frac{b}{a} \qquad (\Omega) \tag{3.15}$$

where $Z_{0,const}$ is the characteristic impedance of vaccuum in [Ω].

3.1.4.2 Low frequencies (LF)

The analytical expressions for capacitance and conductance of the coaxial cable remains the same at all frequency ranges. The resistance and inductance at low frequency range is obtained from [10].
The resistance per unit length is given by (3.16)

$$R = \frac{1}{\sigma_c \pi}(\frac{1}{a^2} + \frac{1}{c^2 - b^2}) \qquad (\Omega/m) \tag{3.16}$$

The inductance per unit length is given by (3.17)

$$L = \frac{\mu}{2\pi}\{ln(\frac{c}{a}) + \frac{2(\frac{b}{c})^2}{1-(\frac{b}{c})^2}ln(\frac{c}{b}) - \frac{3}{4} + \frac{\frac{c^4}{4} - c^2b^2 + b^4(\frac{3}{4} + ln(\frac{c}{b}))}{(c^2-b^2)^2}\} \qquad (H/m) \tag{3.17}$$

The characteristic impedance of the cable is given by (3.18)

$$Z = \sqrt{\frac{R + j\omega L}{G + j\omega C}} \qquad (\Omega) \tag{3.18}$$

3.1.5 Analytical representation of twinaxial cables

A complete mathematical representation for twinaxial cables were not found in literature for different frequencies. Hence the FEM simulations were only compared with measurements.

3.2 Measurement set-up of coaxial and twinaxial cables

The impedance parameters of coaxial and twinaxial cable are measured by using a vector network analyzer (VNA). This section will describe about the VNA, the test setup and the measurement method adopted in this thesis. The measurement results are discussed in the next chapter.

3.2.1 Vector Network Analyzer

A VNA from Omicron is used for measurements in this work. The VNA provides accurate impedance measurements from mΩ to MΩ with a wide frequency range of 1 Hz to 50 MHz. Unlike the bulky conventional measuring equipments, the modern VNA is compact and portable [14].

The architecture of VNA comprises of a signal source which provides a sinusoidal sine wave and two channels; one channel is used for providing a reference and the other channel for picking up measurements. It provides flexibility of connecting the reference channel either internally or externally to the source signal. The architecture of VNA is indicated in Figure 3.1, where 'S' is the source signal, 'A' is the reference channel connected internal/external to the source signal and 'B' is the measurement channel.
The VNA provides flexibility of measurements for different applications such as:

- Gain/Phase (transfer function) measurements
- Transmission/Reflection measurements
- Impedance measurement

In this thesis, the measurements were carried out for the above mentioned applications. The source of the VNA has a resistance of 50Ω and connections were done with 50Ω BNC cables. Basically, the VNA measures the voltage at Channel B for a specific or range of frequencies and compares it with the sinusoidal wave generated by the source in order to derive the magnitude and phase of the measured signal.

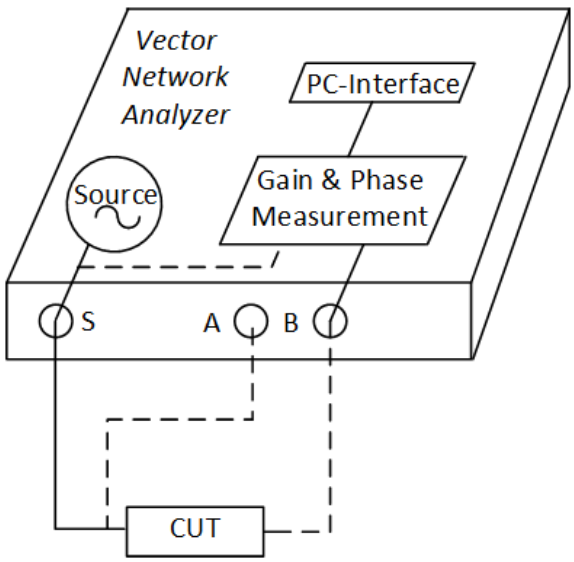

Figure 3.1: VNA architecture and its connection to CUT

3.2.1.1 VNA principles of operation

The measurement data that is obtained from reference channel 'A' and measurement channel 'B' is used to calculate the gain and phase of the CUT.
The VNA provides a sinusoidal voltage at the output 'S', measures the voltages at the input of channels A & B, and delivers a voltage ratio of V(Channel A)/V(Channel B) as given in equation 3.19

$$\underline{H(f)} = \frac{\underline{V_{ChannelB}}}{\underline{V_{ChannelA}}} = amplitude.e^{j.phase} \tag{3.19}$$

As mentioned above, VNA provides flexibility of connecting the reference; however, using channel 'A' as internal reference is the available default configuration. Even

though, measurements with external referencing of 'A' are correct, internal referencing connection liberates the user for the need of an additional cable connected to reference channel 'A'. For measurements in a large frequency range, 'frequency sweep' option of VNA is used. Prior to carrying out any measurements, the VNA is calibrated so as to eliminate side effects of measuring the CUT such as offsets or capacitive coupling effects.

3.2.2 Measurement Method for Coaxial Cable

A simple open and short circuit method is used for impedance measurement of cable. In the former method, copper conductor and shield at one end are open, while in the latter method copper conductor and shield are shorted. R and L can be measured from short circuit measurement, while from open circuit measurement G and C can be measured.

3.2.2.1 Short circuit measurement

The VNA is capable for making accurate measurements ≈ above 25 mΩ. Since the resistance of the cable is much lower than that, certain arrangements had to be made to measure such low resistance. Short circuit measurements were done by an 'ultra low impedance measurement method' [16]. The ultra low impedance measurement is different from the normal short circuit method in a way that common mode transformer is connected between Channel 'B' and the CUT so as to eliminate ground loops and obtain precise measurements, while the other end of the cable remains shorted. In Figure 3.2, a coaxial cable short circuit is indicated by connecting the shield to the conductor.

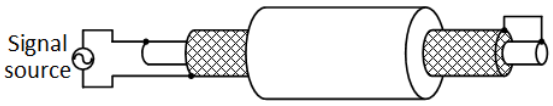

Figure 3.2: Coaxial cable short-circuit

3.2.2.2 Open circuit measurement

During the open circuit measurements, a source signal is applied at one end of the cable, while at the other end, the shield and conductor are left unconnected as indicated in the Figure 3.3

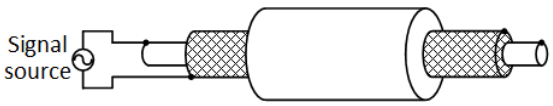

Figure 3.3: Coaxial cable open-circuit

As mentioned earlier, the internal resistance of the source is 50Ω, and hence the VNA is not efficient enough to provide measurements for high impedance. By using an external measurement bridge, the VNA can measure impedance values until several MΩ. The components in the bridge are indicated in Figure 3.4. An impedance

bridge calibration is carried out before performing measurements to compensate for the bridge parasitics.

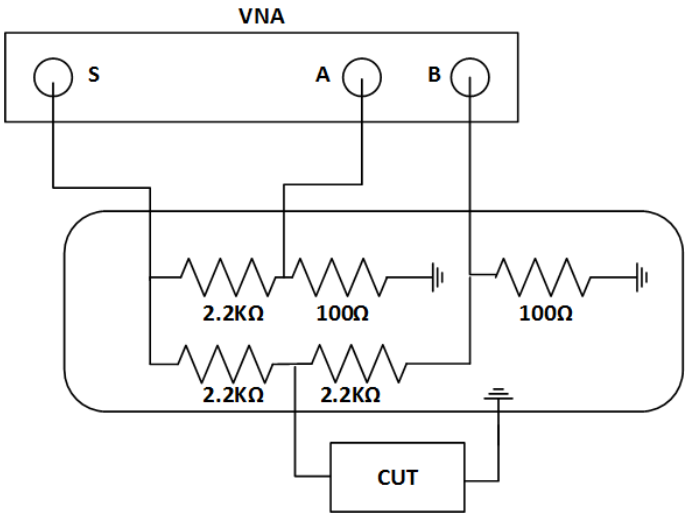

Figure 3.4: high impedance bridge measurement setup

3.2.3 Measurement Method for twinaxial

The same measurement technique of open and short circuit as in the coaxial cable in section 3.2.2, is adapted for twinaxial cable. Since the twinaxial cable has two conductors enclosed by a common shield, the source signal has to be split to both the conductors. This can be done with the help of a common mode transformer connected at the end of source signal. The important difference that has to be focused on is that, in a twinaxial cable, neither of the signals that are supplied to the two conductors are referenced to a ground unlike a coaxial cable.

3.2.3.1 Short circuit measurement

Short circuit measurements were done by connecting a common mode transformer between the source signal and the CUT so as to apply equal and opposite voltages to the two conductors, while the other end of the conductors remained shorted. In Figure 3.5, a twinaxial cable short circuit is indicated by shorting the two conductors while the shield is left open at both ends.

Figure 3.5: twinaxial cable short-circuit

3.2.3.2 Open circuit measurement

The twinaxial cable consists of capacitance between conductor and conductor; and capacitance between conductor and screen. The capacitance between conductor

and screen is measured as shown in Figure 3.6. The conductors are shorted and capacitance is measured between one of the conductor and screen. The other end of the cable is left open. The capacitance is obtained from (3.20)

$$C_{M1} = 2C_{c/s} \tag{3.20}$$

where C_{M1} is the measured capacitance and $C_{c/s}$ is capacitance between conductor and screen.

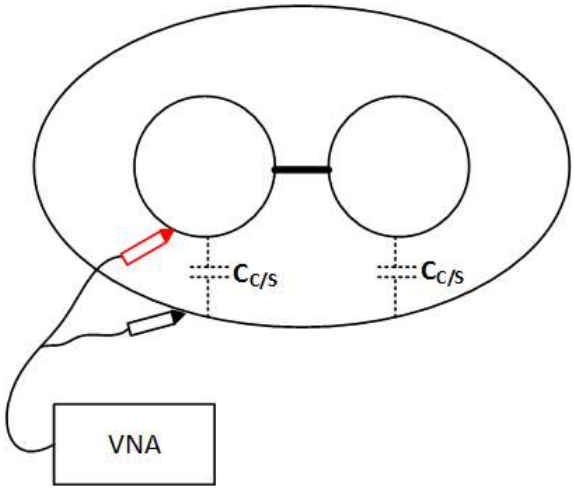

Figure 3.6: Capacitance between conductor and screen

The capacitive coupling between the conductors is measured as shown in Figure 3.7. One of the conductor and shield are shorted and capacitance is measured between the conductors. The other end of the cable is left open. The capacitance is obtained from (3.21)

$$C_{M2} = C_{c/c} + C_{c/s} \quad ; \quad C_{c/c} = C_{M2} - C_{c/s} \tag{3.21}$$

where $C_{c/c}$ is the capacitive coupling between the conductors.

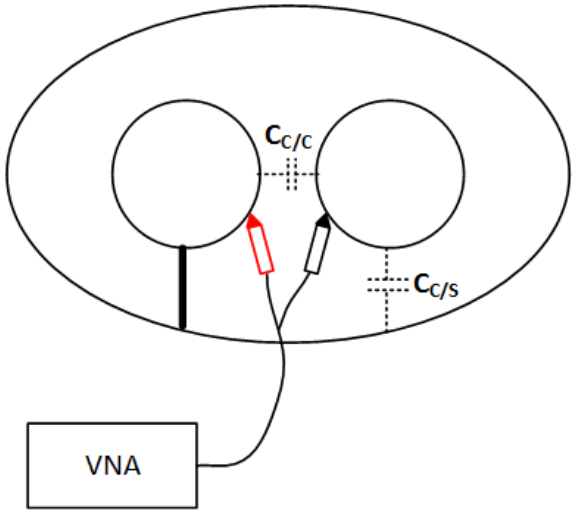

Figure 3.7: Capacitance between conductor and conductor

3.2.4 Measurement method for parallel coaxial and twinaxial cable

This section will describe the measurements carried out with a single coaxial and twinaxial cable at different heights above the copper frame. Also, this section includes the measurements conducted for coaxial cables with different distances between them. Best efforts were made in the laboratory setup to follow similar arrangement of cables and the chassis in a bus.

Both sides of shield were grounded and the far end of the conductor is shorted to frame to obtain inductive coupling between conductor and frame. The conductor extended beyond the shield for both coaxial and twinaxial cable to make connection from VNA.

To obtain capacitive coupling between the coaxial cable and the copper frame, the farther end of the conductor is kept open and shield is grounded at both ends.

4

Analysis of results

4.1 FEM & Measurement

This section begins by analyzing the FEM and analytic results. Also, comparisons were made between laboratory measurements and FEM results for cable parameters i.e. R,L,C. These analysis and comparisons were done for both coaxial and twinaxial cables.

This section also discusses the inductive and capacitive coupling measurement results between coaxial cable and copper frame at different heights, and between two parallel coaxial cables. The variation in inductance due to single grounding and double grounding of the shield is also discussed.

4.1.1 Coaxial cable FEM results

The Figures 4.1, 4.2, 4.3 and 4.4 shows the comparison of FEM and analytic results modelled from Section 3. It can be seen that the FEM results for different parameters in the cable match very closely with the analytical expressions. This validates the TEM theory and is used as a base to compare measurements.

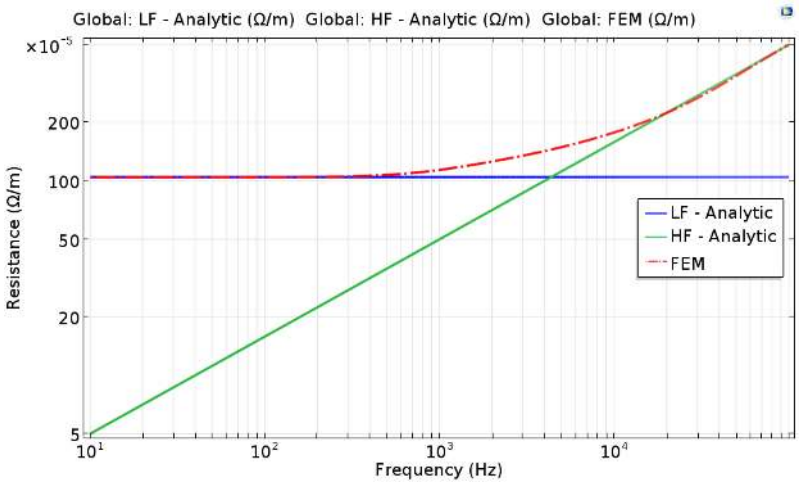

Figure 4.1: Analytical and simulated result for resistance of 50 mm^2 cable

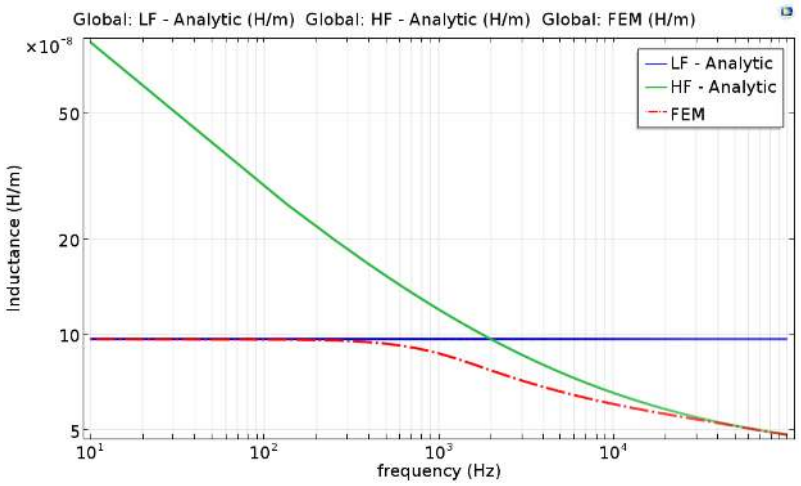

Figure 4.2: Analytical and simulated result for inductance of 50 mm^2 cable

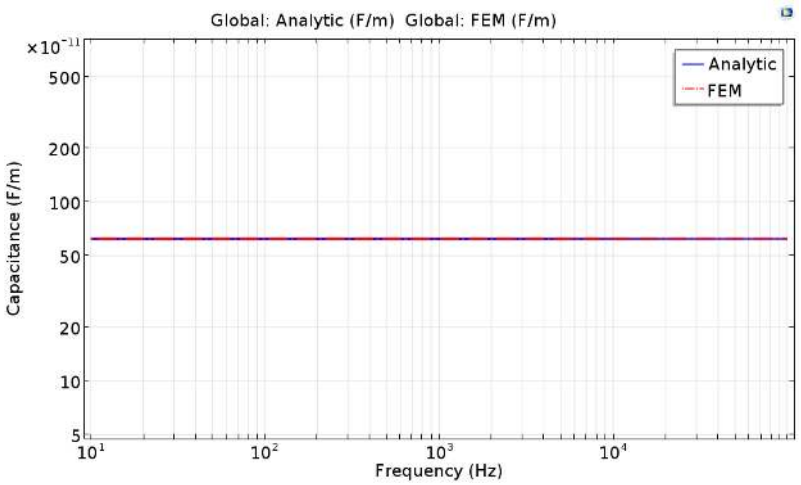

Figure 4.3: Analytical and simulated result for capacitance of 50 mm^2 cable

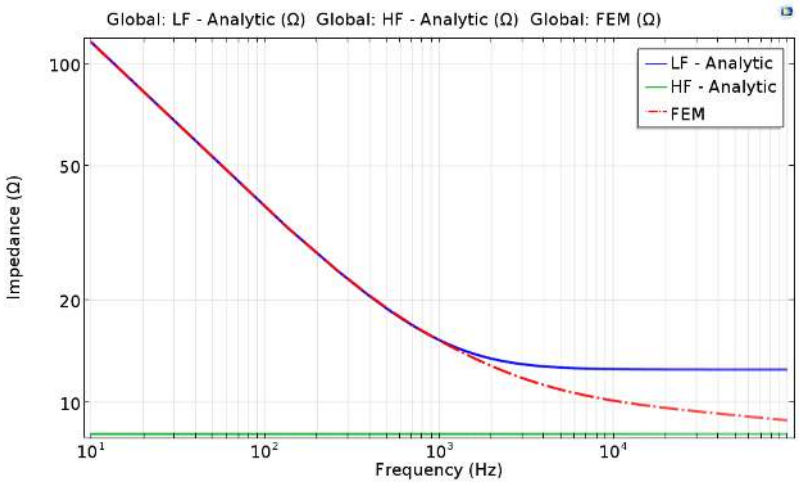

Figure 4.4: Analytical and simulated result for impedance of 50 mm^2 cable

4.1.2 Comparison of FEM and Measurements

The Figure 4.5 shows the comparison of measurement and simulated results for resistance and inductance in a 50 mm^2 cable. It can be seen from the figure that there is an offset between measurement and full FEM. This is due to the assumption made in FEM that the shield is solid and the shield completely encloses the conductor. Since a solid shield has lower resistance because of large cross sectional area, the resistance obtained from FEM is lower than measurements. In order to verify that the offset is because of the shield, the resistance of the shield is measured and added with the resistance of the conductor from FEM simulations. The result is shown as hybrid FEM in Figure 4.5. Now it can be seen that the hybrid FEM result is very close to measurements in the mid frequency range. At higher frequencies the behaviour of solid shield is different than that of a braided shield and hence the exponential increase in slope [1].

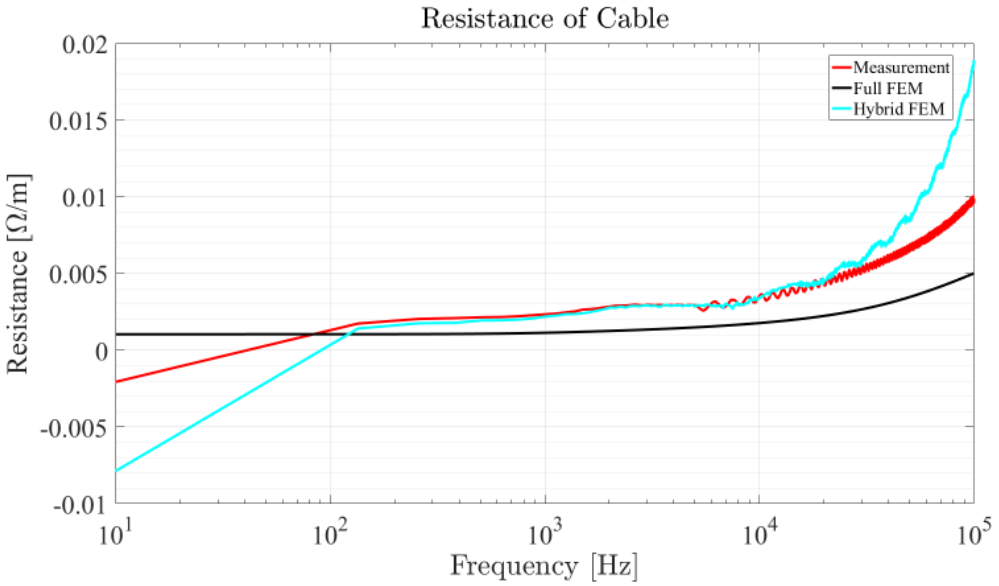

Figure 4.5: Comparison of resistance for 50 mm^2 cable

The Figure 4.6 also shows an offset between the inductance obtained from FEM and measurements. This offset is explained from Figure 2.7 in Section 2.3.2.1. It can be seen in Figure 2.7 that there exists a mutual inductance between the shield and conductor due to the holes in the braided shield. Again due to the assumption made in FEM that the shield is solid and there is a current flowing in opposite direction of same magnitude, the mutual inductance between the shield and conductor is zero. Since the mutual inductance in FEM is zero, the inductance obtained from FEM is lower than measurements. But in measurements there exists a mutual inductance which is equal to the self inductance of the shield [1]. Certain attempts were made to measure the inductance of the shield but satisfactory results were not obtained.

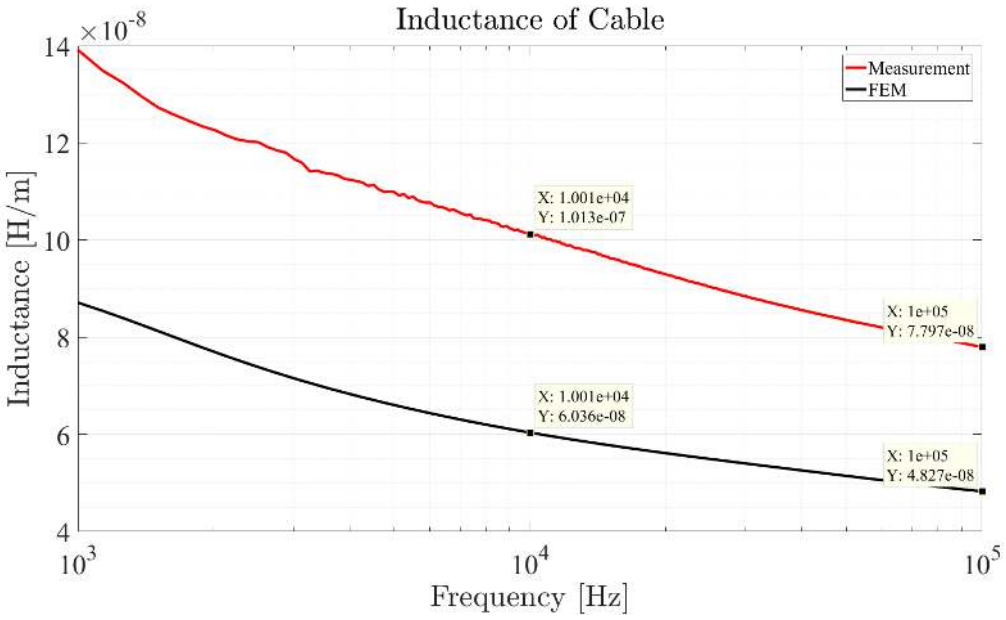

Figure 4.6: Comparison of inductance for 50 mm^2 cable

The Figure 4.7 shows the capacitance values between FEM and measurements. Technically, in the coaxial cable, the copper conductor and the shield are analogous to a parallel plate capacitor. The capacitance between a parallel plate capacitor is directly proportional to permittivity of the material and inversely proportional to distance. Since the material properties of the dielectric were not given from the supplier, a standard value for the relative permittivity is assumed for the dielectric in FEM which is 2.25 – j*0.01. The small difference in capacitance value can arise due to mismatch in permittivity and also, the values are affected by the environment since the shield is not properly terminated.

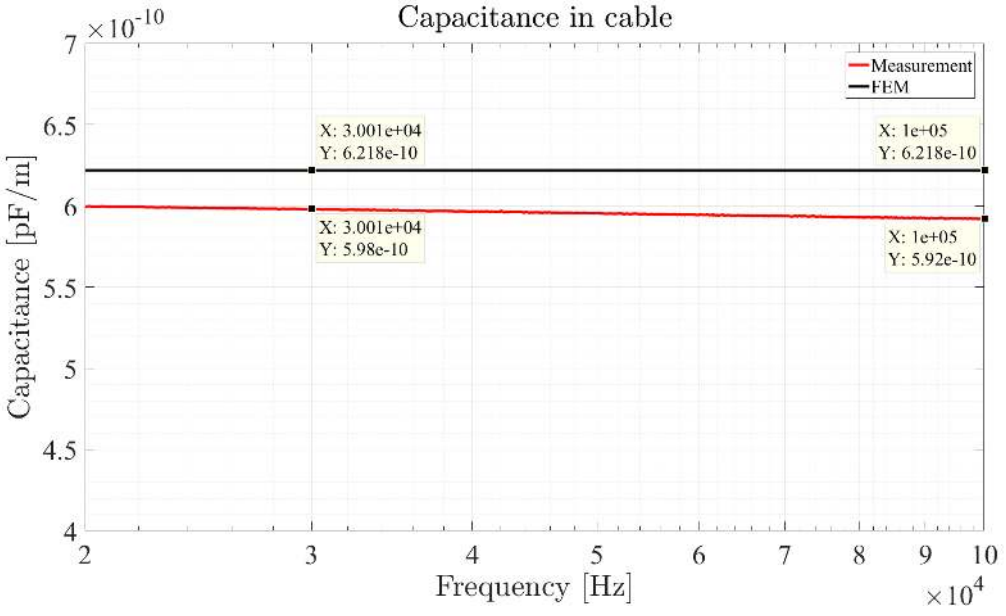

Figure 4.7: Comparison of capacitance for 50 mm^2 cable

4.1.3 Twinaxial cable results

The results from FEM were only compared with measurements, since there is no well defined expressions for twinaxial cables. The Figure 4.8 shows the comparison of resistance for 2x4 mm^2 between FEM and measurement. It can be seen that the results converge closely at low and mid frequency ranges. But at higher frequencies >50kHz, the increase in slope in measurements is higher than FEM. This is due to the skin effect arising from connecting cables and connectors.

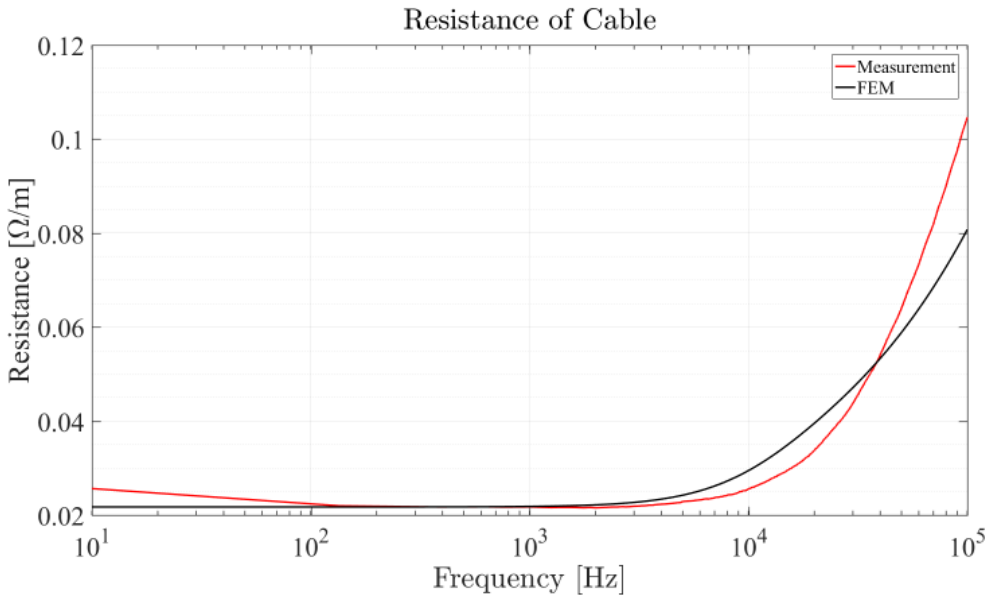

Figure 4.8: Comparison of resistance for 2x4 mm^2 cable

The Figure 4.9 shows the comparison of inductance in 2x4 mm^2 between FEM and measurements. The inductance at lower frequencies were ignored since there is no inductance and omega is the dominating term. The results were analyzed only above 8kHz where the inductance is dominating. It can be seen that the measurements match closely with FEM simulations. The error between FEM and measurements at higher frequencies is less than 20%. This difference is due to the stray inductance present in the connecting cables. Since there is no involvement of the shield in twinaxial cable, there is no offset in the inductance value as in case of coaxial cable.

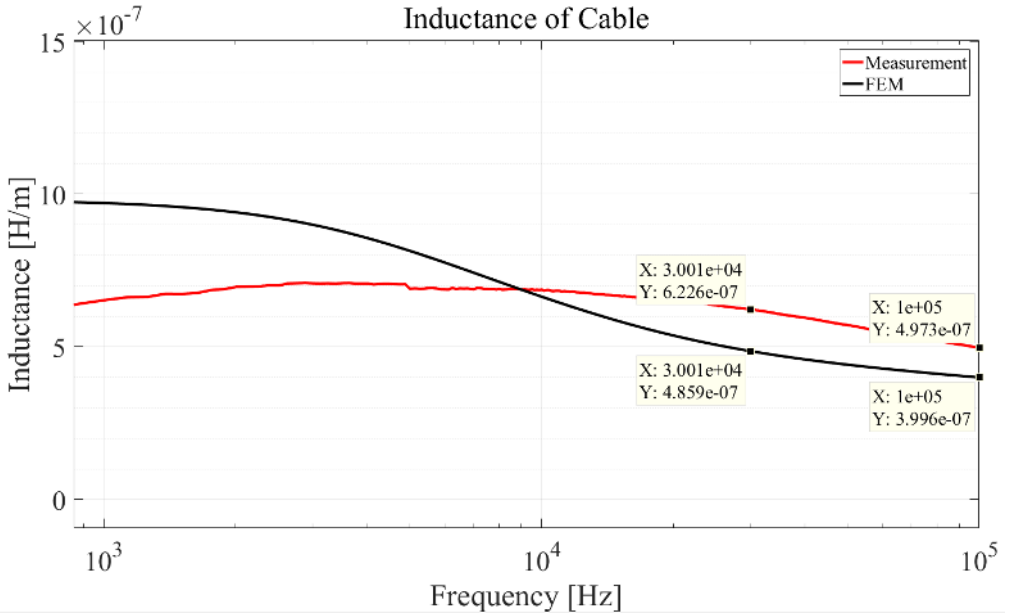

Figure 4.9: Comparison of inductance for 2x4 mm^2 cable

Table 4.1 shows the comparison of capacitance values between FEM and measurements. The capacitance between conductor to screen and conductor to conductor is obtained using the (3.20) and (3.21). The difference in capacitance values is explained in the same way as it was done for coaxial cables. Since capacitance is constant at all frequencies, the values were obtained at 100kHz where the coupling was purely capacitive. And also due to lack of computation power, the capacitance computed from admittance matrix in FEM were only evaluated for one frequency rather than performing a frequency sweep.

Table 4.1: Capacitance comparison for 2x4 mm^2 cable

Nom. Capacitance	**FEM**	**Measurements**
Conductor and screen (pF/m)	355.61	295.5
Conductor to conductor (pF/m)	37.9	75.9

4.1.4 FEM results based on placing of cables

4.1.4.1 Coaxial cables

The cable parameters for 600 V network were analyzed here based on their placing. Figure 4.10 shows the loss parameters for various separation distances between the cables. It can be seen that the resistance, inductance and capacitance values are exactly twice that of single 50 mm^2 coaxial cable (now there is two parallel cables). Because of the assumption made for shield stated in previous sections, the electric fields and magnetic fields are totally compensated within a single cable itself. In other words, due to grounding of the shield, the electric fields are compensated and

due to the current flowing in the shield, the magnetic fields are also compensated. Hence there exists no coupling parameters between the cables or with the iron chassis. Due to lack of computational power only certain frequencies were evaluated.

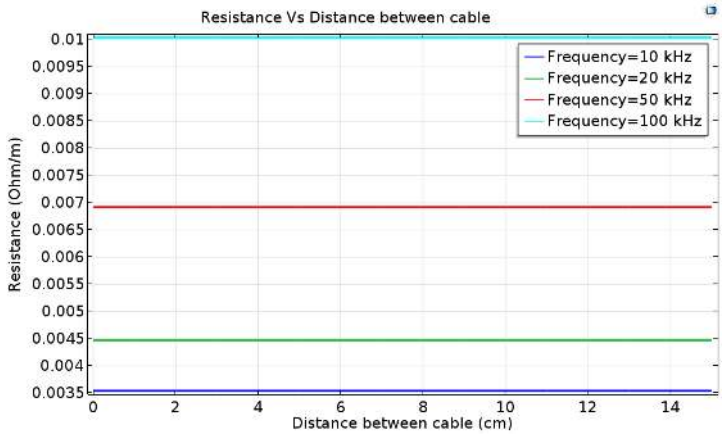

(a) Resistance of the system when cables are separated

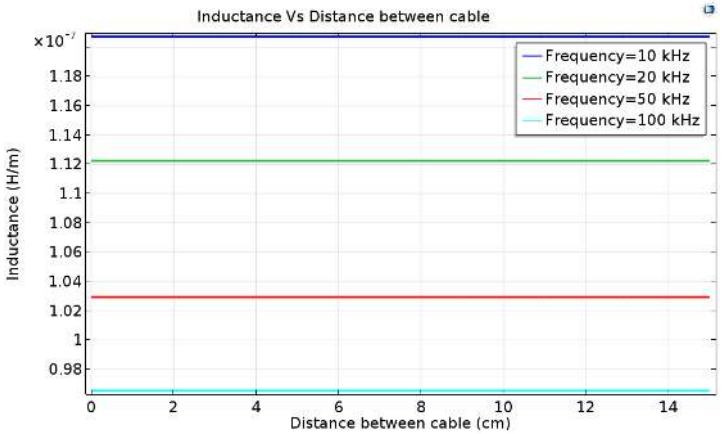

(b) Inductance of the system when cables are separated

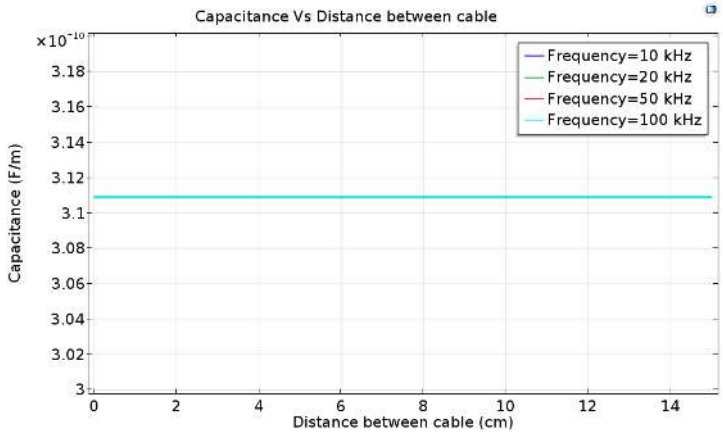

(c) Capacitance of the system when cables are separated

Figure 4.10: Loss parameters for various distances between the cables

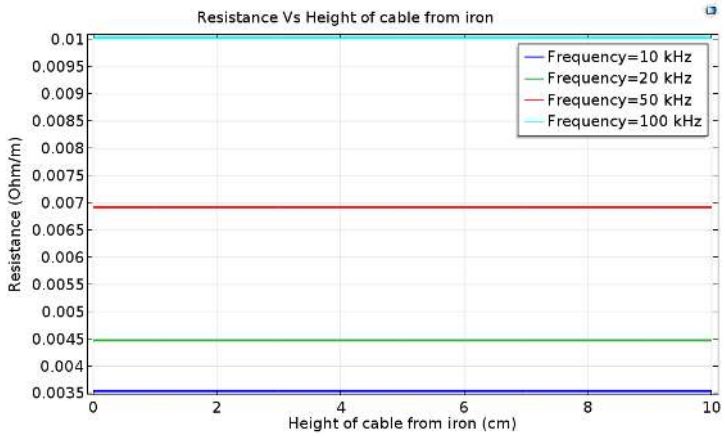

(a) Resistance of the system when cable and chassis are separated

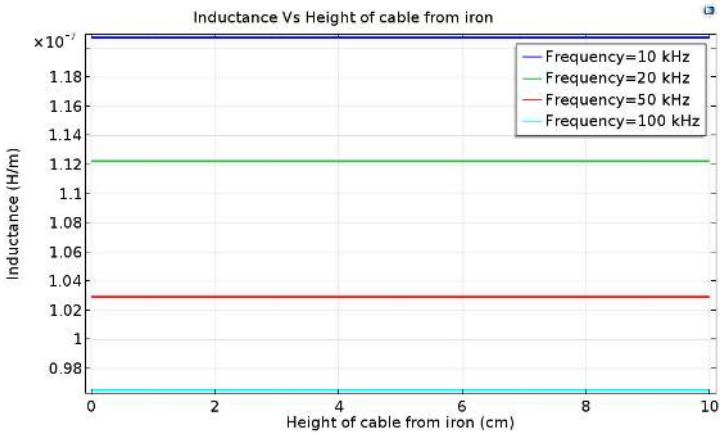

(b) Inductance of the system when cable and chassis are separated

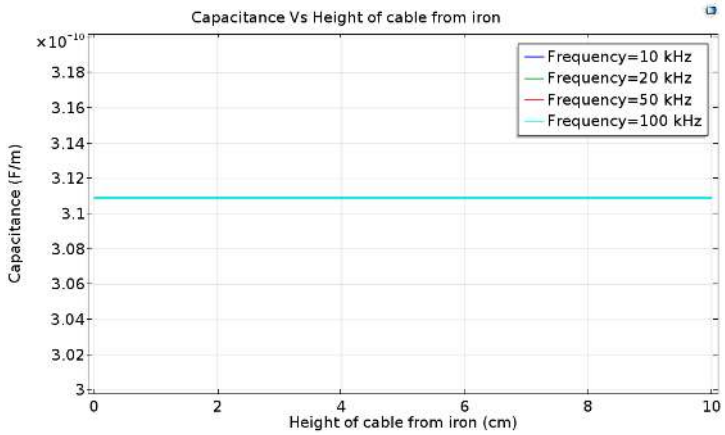

(c) Capacitance of the system when cable and chassis are separated

Figure 4.11: Loss parameters for different distances between cable and chassis

The same parameters were analyzed for different heights of the cables from the iron chassis. Figure 4.11 shows the loss parameters for cable when they are placed at

different heights from the chassis. It can seen be as well that the values are exactly twice that of single 50 mm^2 coaxial cable. The explanation is similar to the one mentioned in the previous paragraph.

4.1.4.2 Twinaxial cables

The same parameters were analyzed for twinaxial cables for different heights from the iron chassis. Figure 4.12 shows the loss parameters for cable when they are placed at different heights from the chassis. It can be seen that the loss parameter values are not affected by the placing of cables at the defined frequencies. This is because the magnetic fields are cancelled due to currents of equal magnitude flowing in opposite directions in the two conductors. The electric fields are also cancelled due to grounding of shields. Since there is no leakage of electric or magnetic fields to couple with the chassis, the impedance is not affected by placing of the cables.

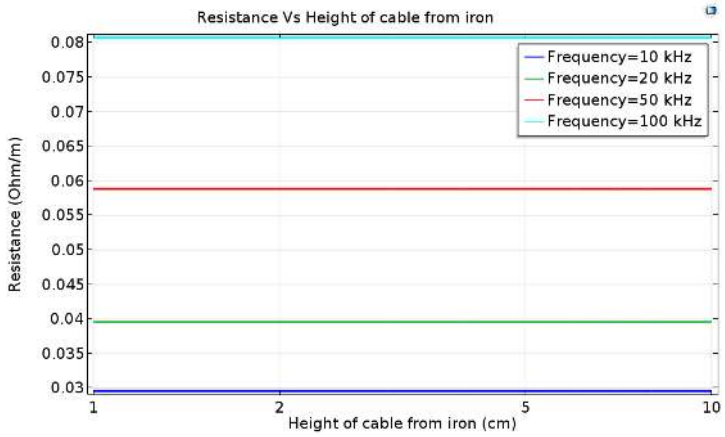

(a) Resistance of the system when cable and chassis are separated

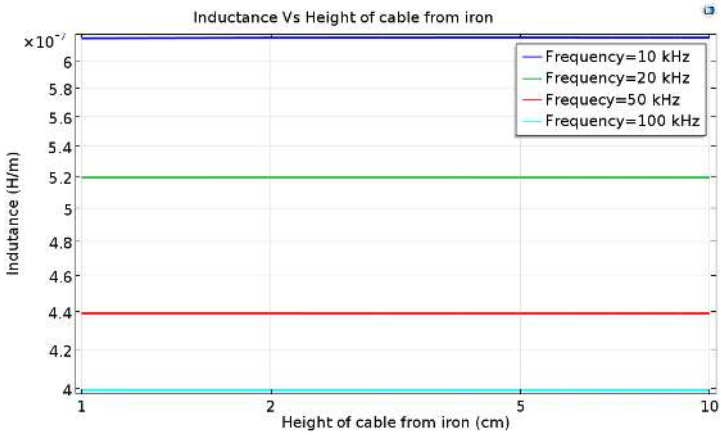

(b) Inductance of the system when cable and chassis are separated

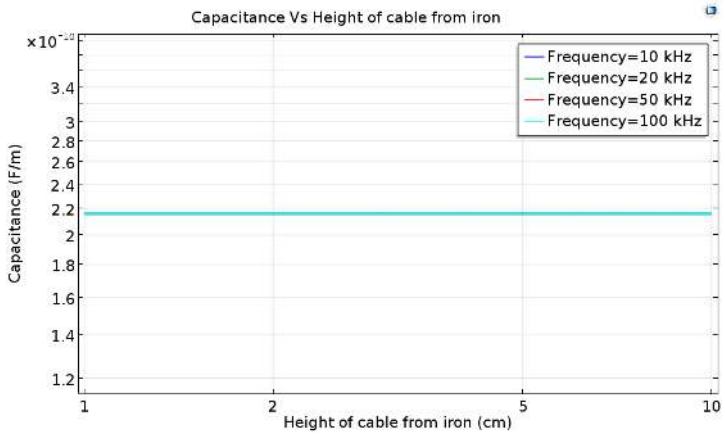

(c) Capacitance of the system when cable and chassis are separated

Figure 4.12: Loss parameters for different distances between cable and chassis

4.1.5 Coaxial cable on a copper frame

4.1.5.1 Inductive coupling between coaxial cable and copper frame

The inductive coupling between the 50 mm^2 coaxial cable at different distances from the copper frame is indicated in Figure 4.13. In the Figure 4.13a, the inductive coupling between conductor/shield to the copper frame is higher than the self inductance of the 50 mm^2 coaxial cable as indicated in Figure 4.6. This difference can be explained by the fact that the copper conductor was not enclosed by shield at the far end of the 50 mm^2 coaxial cable. So, the copper conductor was simply facing the copper frame. Also, it is observed from Figure 4.13a that, as the distance between the coaxial cable and copper frame is increased, the inductive coupling increases. This can be described by visualizing the copper conductor and frame as two parallel wires and the inductance is calculated by the equation 4.1,

$$L = 0.21ln\frac{b}{a} \tag{4.1}$$

where 'b' is the distance between the copper conductor and frame, and 'a' is the radius of the conductor. It is also noted from Figure 4.13a that, after a certain increase in distance between copper conductor and frame, inductive coupling saturates; this is due to the fact that magnetic field weakens as the copper conductor and frame are moved apart.

Figure 4.13b, indicates the inductive coupling between shield and the frame at different distances. By comparing Figure 4.13a and Figure 4.13b, it is observed that inductive coupling between conductor and frame is higher than the inductive coupling between shield and frame. The higher measurement values were due to the fact that, the shield did not enclose the conductor completely; due to which it picked up noise voltage from the copper frame and conductor which is in series to the source signal. A smaller inductance result would have been obtained if the shield had completely enclosed the conductor. This ensures that, a shield i.e, grounded at both the ends, carries the return current equal and opposite to that in the conductor; the opposite field generated in the shield cancels the magnetic field generated by the current in the conductor and hence there are no fields external to the cable. Also, a shield can fully provide its magnetic shielding capability, if it is terminated by a 360 degree contact to the copper frame via a connector [1].

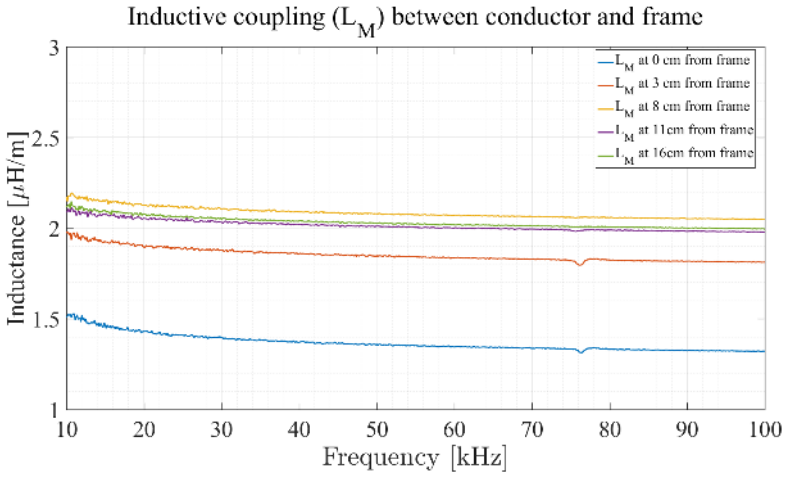

(a) Inductive coupling between the copper conductor and copper frame

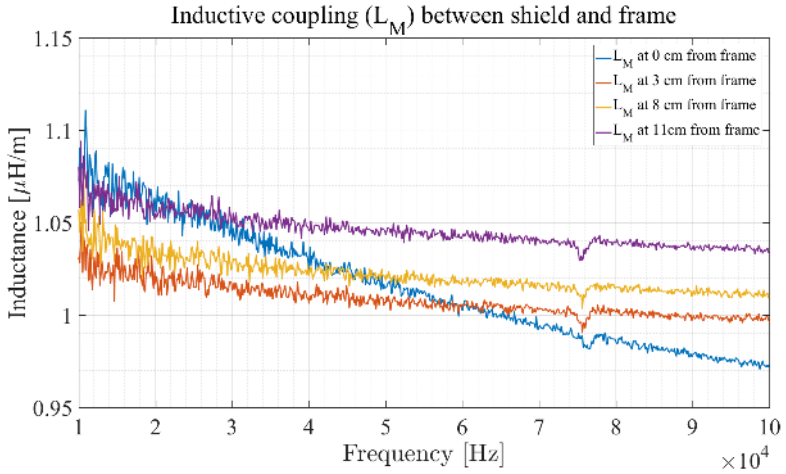

(b) Inductive coupling between the shield and copper frame

Figure 4.13: Inductive coupling between copper conductor and frame, shield and frame with both ends of shield grounded at different heights from the frame

Figure 4.14 indicates inductive coupling between the copper conductor and frame with the grounding of the shield at the source end. These results were compared with the Figure 4.13a in which the shield was grounded at both the ends. It is observed that inductance between conductor and frame in case of a double grounded shield is lower than single grounded shield. This is because at higher frequencies, the ungrounded end of the shield behaves as an antenna and couples the inductance to the frame.

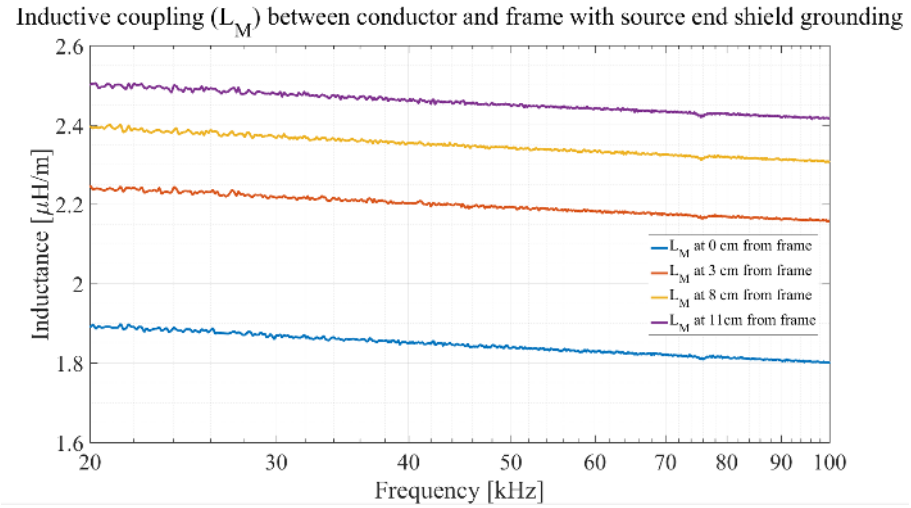

Figure 4.14: Inductive coupling between the copper conductor and frame with source end shield grounding

4.1.5.2 Capacitive coupling between coaxial cable and copper frame

Figure 4.15 indicates the capacitive coupling between copper conductor and frame, at varying distances from each other. It is observed that, the capacitance values remained constant for varying distances from the frame i.e. electric fields remained constant between the conductor and frame, and also it is closer to the capacitance value of the cable by itself. This is because the conductor is not being completely enclosed by the shield, and the conductor basically sees the copper frame which is similar to the measurement setup made in section 3.2.2.2. Also, the noises recorded in the measurements are because of the noise voltages picked up by the conductor from the frame and shield.

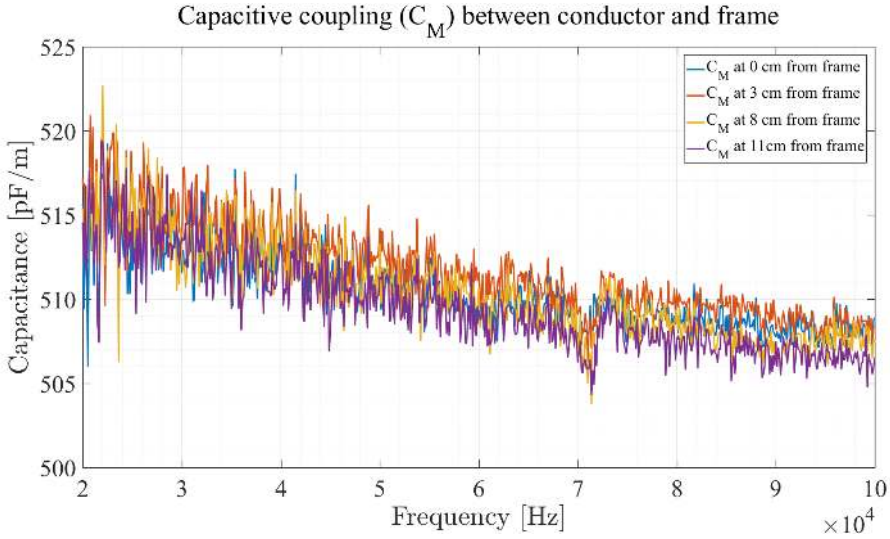

Figure 4.15: Capacitive coupling between conductor and frame, with both ends of shield grounded, at different heights from the frame

4.1.6 Two parallel coaxial cables

Figure 4.16 indicates the inductive coupling of two coaxial cables at varying distances between them. It is noted that inductance between two coaxial cable increases as distance between them is increased. This behaviour can again be explained by visualizing the two cables as two parallel wires, with inductance between them expressed by (4.1).

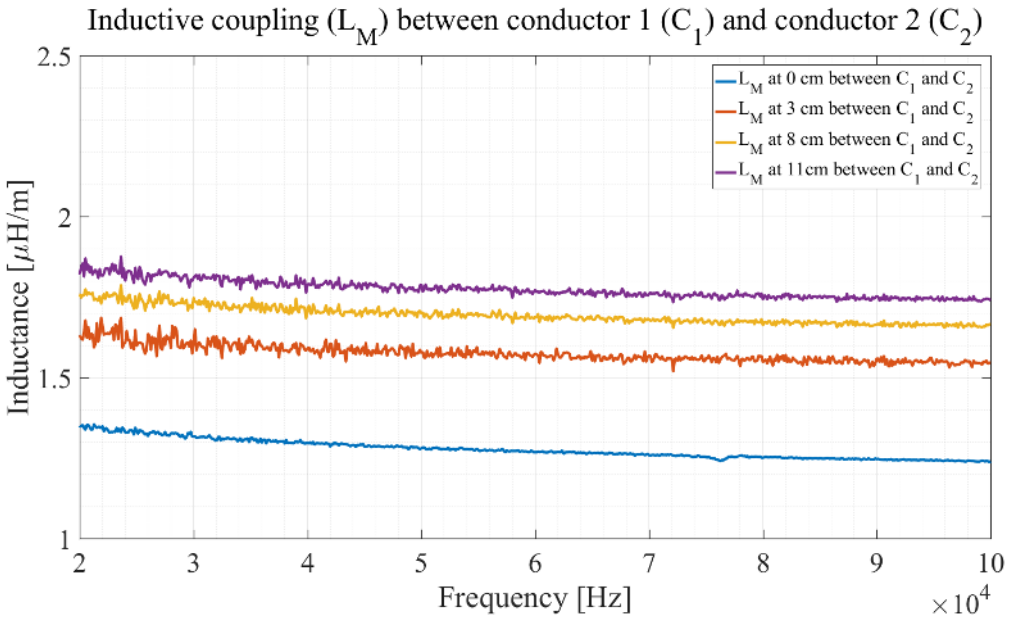

Figure 4.16: Inductive coupling of two coaxial cables for varying distances between them

4.1.7 Twinaxial cable on a copper frame

4.1.7.1 Inductive coupling between twinaxial and copper frame

Figure 4.17 shows the inductive coupling between a twinaxial cable and copper frame with varying heights between them. It can be seen that the values remain pretty constant at different heights. Since a twinaxial cable has two conductors enclosed by a common shield, the magnetic fields generated from the current flowing in one conductor is cancelled by the magnetic fields generated from current of same magnitude flowing in opposite direction in the return conductor. The small amount of noise observed in the figure is due to grounding of shield in both the ends. Since the magnetic fields are compensated by the two conductors, grounding the shield on both ends induces a noise voltage due to the current flowing through the ground loop. This noise voltage coincides with the magnetic fields creating additional noise.

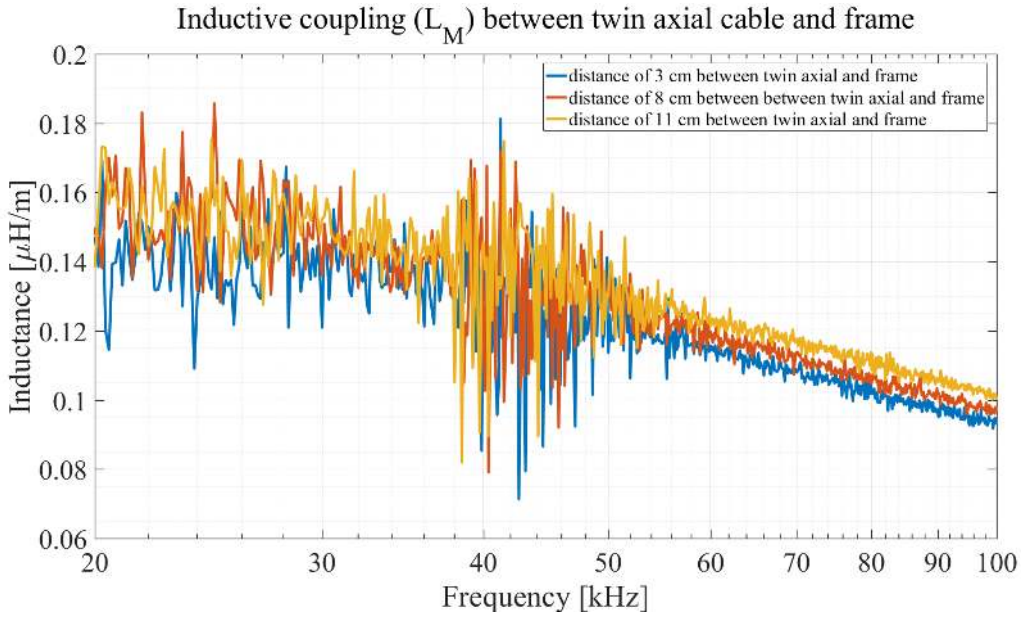

Figure 4.17: Inductive coupling between a twinaxial cable and copper frame with varying heights between them

4.1.7.2 Capacitive coupling between twinaxial and copper frame

The Figure 4.18 shows the capacitive coupling between twinaxial cable and the copper frame. It can be seen that the coupling is independent of the placement but has a higher value. This is again because of improper shield termination explained in previous sections.

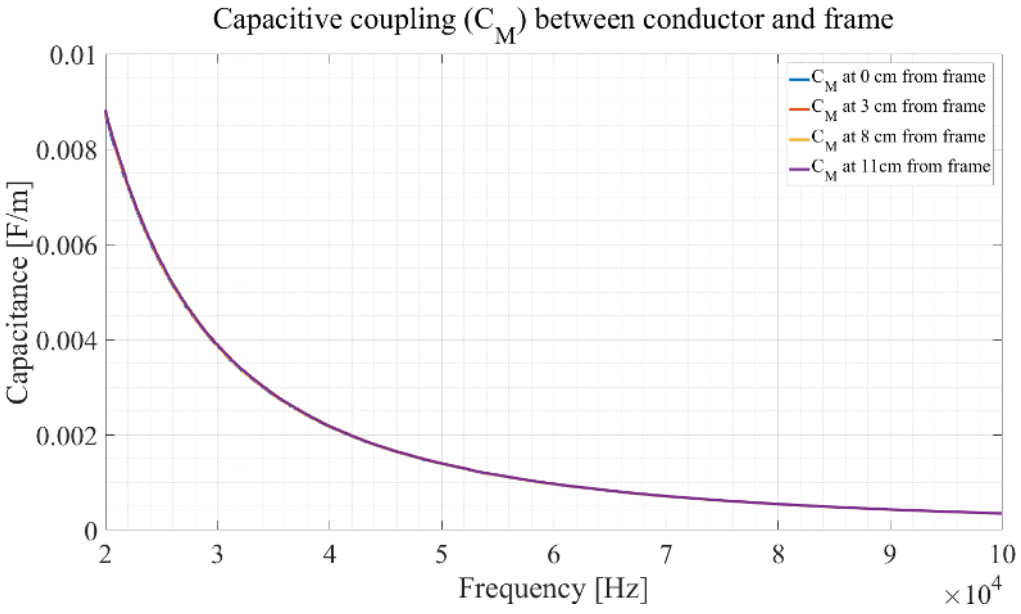

Figure 4.18: Capacitive coupling between a twinaxial cable and copper frame with varying heights between them

4.2 Measurement results from a bus

4.2.1 Coaxial Cable

The Figure 4.19 shows the comparison of inductance between results obtained in vehicle, FEM and lab. Measurements were performed on two 50 mm^2 coaxial cable connecting the HEV junction box to the battery. It can be seen that the results from the vehicle are closer to FEM than obtained from lab. This is due to the fact that the shield was not accessible in the vehicle, the measurements were made between two conductors. Hence the inductance values obtained were the inductance's of two conductors without the inclusion of the shield. This is similar in FEM where the conductor is solid and the shield is also a solid conductor. The total inductance is the combination of conductor and solid shield. At higher frequencies, it can be seen that the inductance in vehicle is lower than FEM. This is because the return path for the signal in FEM is the shield which has lower cross sectional area compared to copper conductor in vehicle. Hence a higher cross sectional area gives a lower inductance as per 4.1.

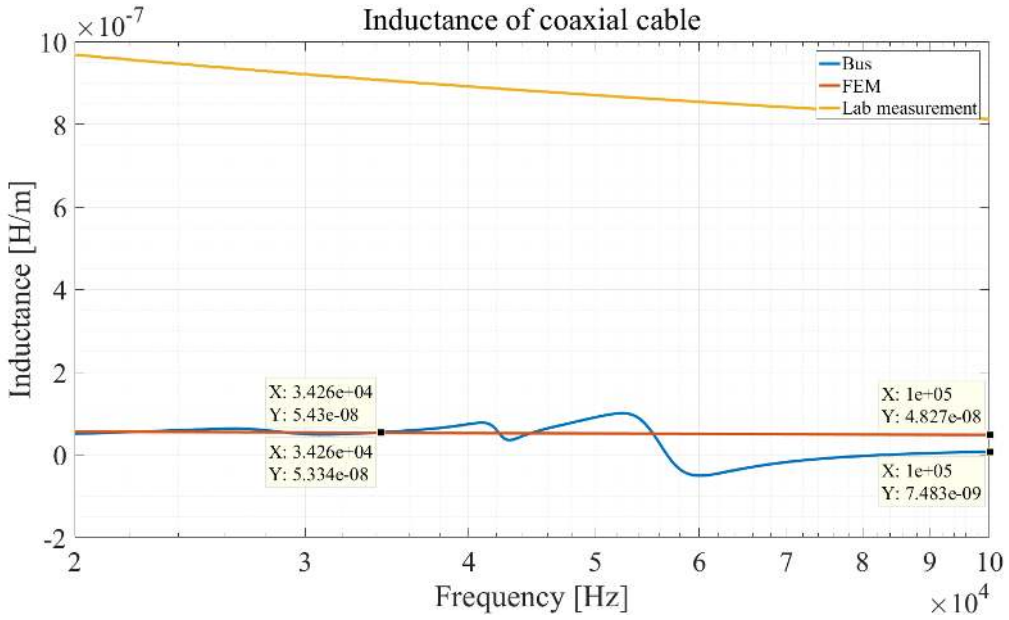

Figure 4.19: Comparison of inductance

As mentioned in theory regarding the working of VNA, the inductance is measured from the phase angle incurred between reflections. Since the cable measured in the vehicle between HEV junction box and battery has terminations and different components (junction box and aluminum plates) in between, the signal is reflected back and forth due to mismatch in impedance. This explains the waveform obtained in bus measurements.
The Figure 4.20 shows the comparison of resistance between results obtained in vehicle, FEM and lab. It can be seen that the results from the vehicle are closer to FEM and lab at frequencies between 100 Hz and 1 kHz. At higher frequencies, the

resistances of terminations and other components rises due to skin effect which can be seen from the reflections.

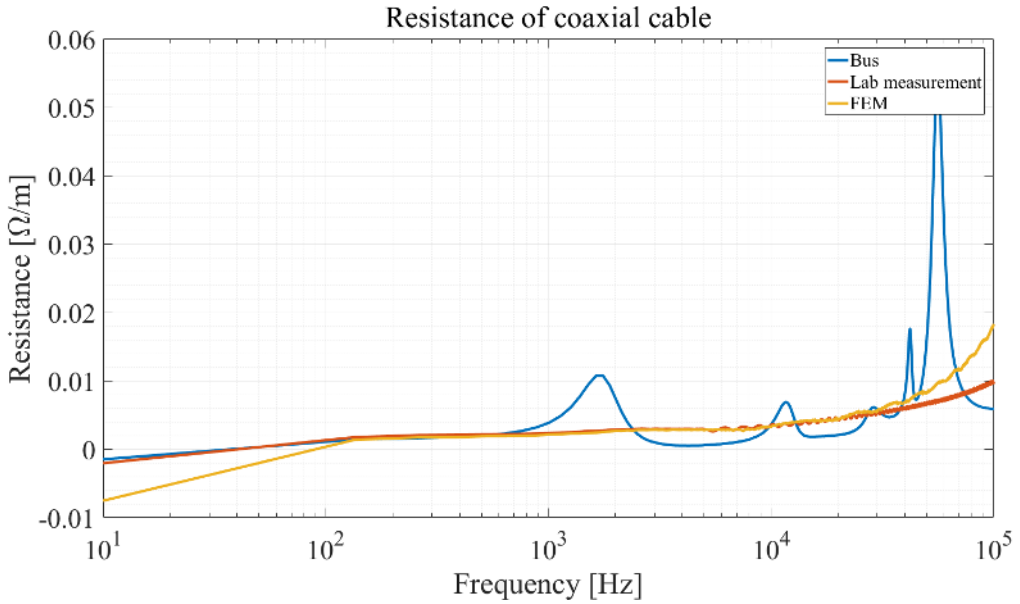

Figure 4.20: Comparison of resistance

The Figure 4.21 shows the comparison of capacitance between results obtained in vehicle, FEM and lab. It can be seen that the results from the vehicle are higher by a magnitude of 10^3 than the lab measurements. The is because the vehicle has capacitors and bleeder resistors connected between the terminals to balance the harmonics in the system.

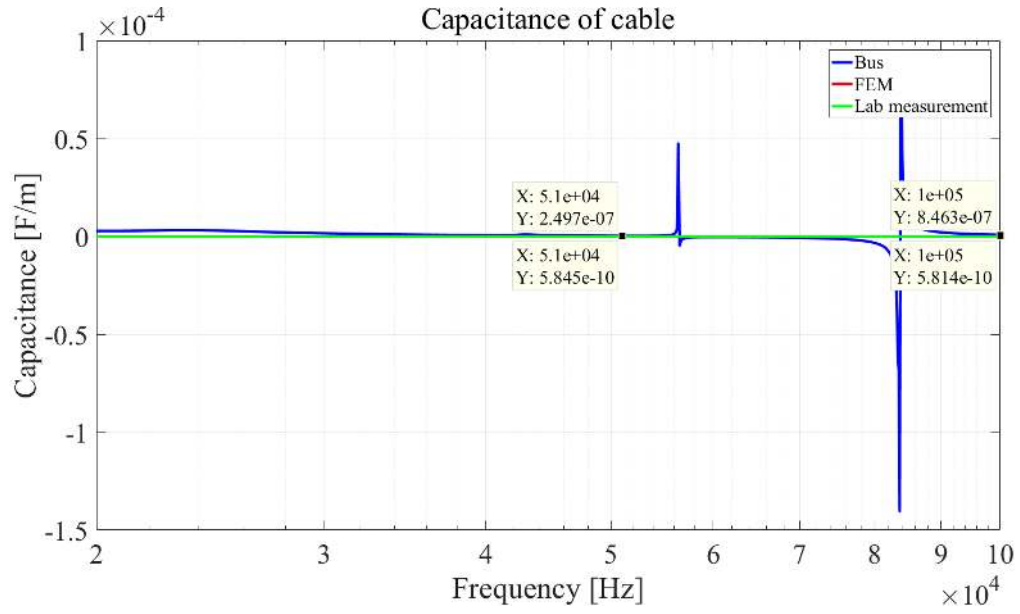

Figure 4.21: Comparison of capacitance

4.2.1.1 Inductive coupling between coaxial cable and chassis

The Figure 4.22 shows the comparison of inductive coupling between conductor and chassis in vehicle and lab measurements. It can be seen that the vehicle has lower inductive coupling compared to the measurement taken in lab. This is because one end of the battery cable had the shield completely enclosing the conductor. In other words, the shield has 360° termination along the circumference of the conductor. Hence the leakage of magnetic fields from the conductor were properly cancelled out by the shield.

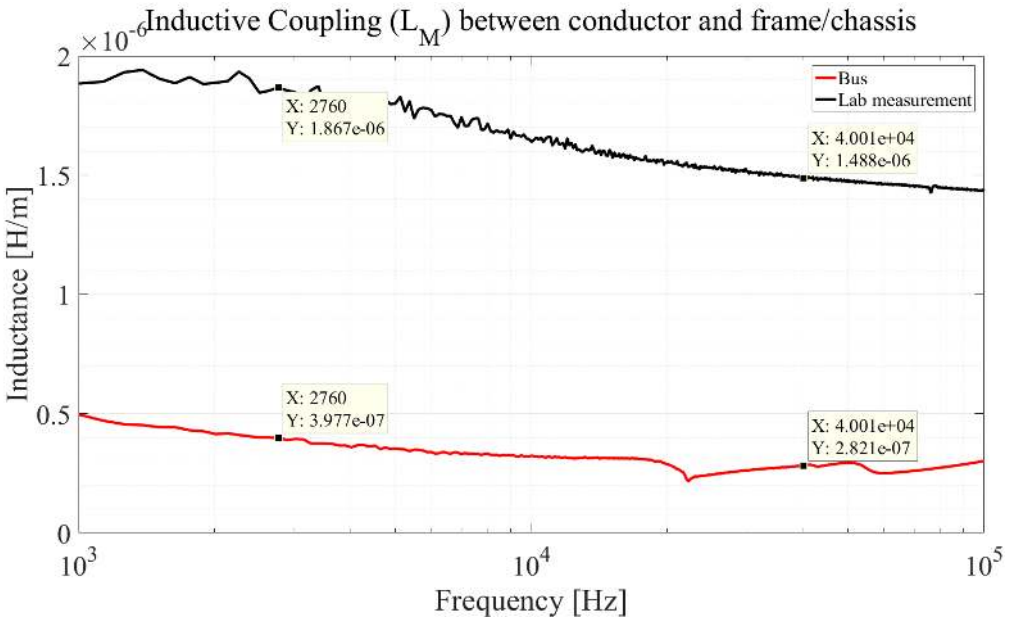

Figure 4.22: Comparison of inductive coupling

4.2.1.2 Capacitive coupling between coaxial cable and chassis

The Figure 4.23 shows the comparison of capacitive coupling between conductor and chassis in vehicle and lab measurements. It can be seen that the vehicle has higher capacitive coupling compared to the measurement taken in lab. This is because there are filter capacitors and bleeder resistors connected between the DC terminals and to the chassis in the vehicle. These filter capacitors are used to filter the harmonics and the charges stored in these capacitors are discharged through the bleeder resistors when the TVS is tuned off.

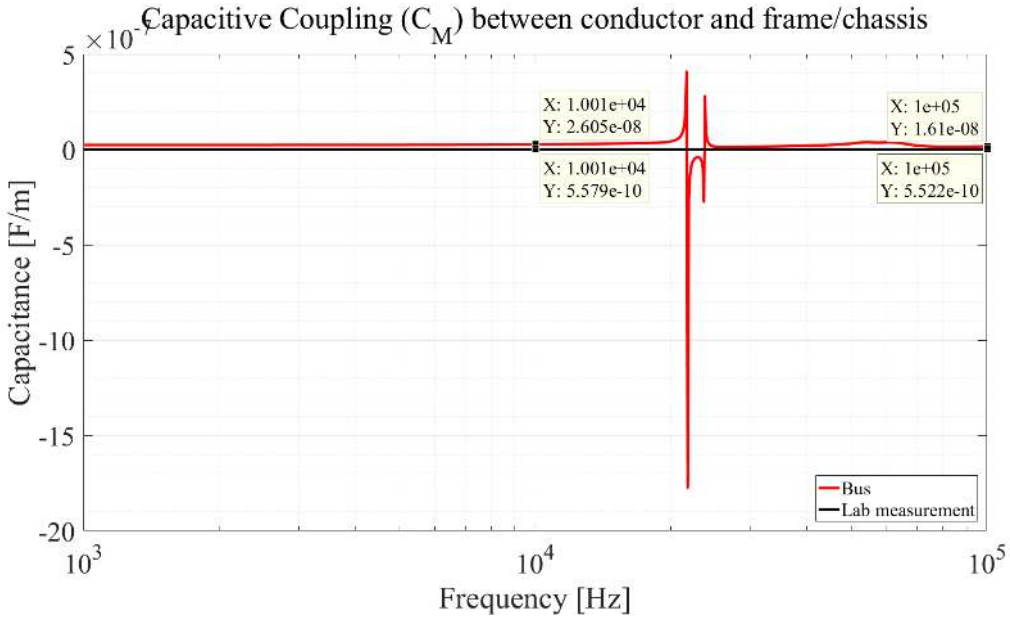

Figure 4.23: Comparison of capacitive coupling

4.2.2 Twinaxial Cable

A comparison was also made for FEM, bus and lab measurement results for twinaxial cable considering impedance parameters i.e. inductance, resistance and capacitance. Also, measurement results were obtained for inductive and capacitive coupling between twinaxial cable and the bus chassis.

Measurements were performed on two 2x4 mm^2 twinaxial cable connecting the HEV junction box to the HVAC. The conclusions drawn by observing results for the above mentioned measurements for twinaxial cable were same as the ones discussed in section 4.2.1

5
Conclusion

5.1 Results from present work

This thesis summarizes the effect of impedance at different frequencies for coaxial and twinaxial cables. These HV cables were modelled in FEM environment. Measurements were carried out in laboratory and a hybrid bus by using a VNA to verify the FEM results. Also, FEM and measurement studies were conducted to study the impedance of these cables based on their placements.

The following observations were made from the comparison of FEM and measurement results of coaxial and twinaxial cables. The offset between the FEM and lab measurement results for resistance and inductance parameters was due to the assumption of solid shield modelled in FEM instead of a braided shield. This offset was verified for the resistance parameter by taking 'Hybrid FEM' results which were close in accordance with the laboratory results. A second observation was that, for a coaxial cable with a braided shield, there exists a mutual inductance between the shield and conductor which is unlike the case for a coaxial cable with a solid shield. For the twinaxial cable, FEM and lab measurement results for impedance parameters were seen to converge closely. The increase in slope for resistance measurement was identified as skin effect and the error in inductance measurement was due to stray inductance arising from cables and connectors. The capacitance parameters were in close accordance with FEM and lab measurements, and remained to be constant at all frequencies.

The impedance of HV cables were also analyzed in FEM and by laboratory measurements based on separation distances between them and for various heights from the iron frame. The following conclusions were made from FEM analysis. Firstly, for coaxial cables separated by different distances and heights from the frame, there existed no coupling between the cables and iron chassis since electric and magnetic field were compensated due to the solid shield. Secondly, for twinaxial cables, it was observed that the loss parameters remained unaffected at different heights due to the cancellation of magnetic fields formed by currents flowing in opposite direction in the twin axial cable conductors. The investigation for the same in laboratory gave insights on the importance of proper shield terminations in a coaxial and twinaxial cable to avoid the mutual coupling between the cable and the copper frame. A study on single and double grounding of shield to the copper frame was also carried out to study the behaviour of inductive coupling between the coaxial cable and frame.

Finally, measurements were carried out in a hybrid bus to validate the FEM and laboratory measurements. For coaxial cable, inductance parameter in bus measurements were in close accordance with FEM results as inductance values were obtained between two solid copper conductors, and at high frequency low inductance is observed in bus measurement due to the higher cross sectional area of the conductor when compared to the shield. The results of bus measurement were close to FEM and lab from 100 Hz to 1 kHz. It was concluded that, at higher frequencies, the high resistance of cable was due to skin effect. The investigations of inductive coupling between coaxial cable and chassis gave low values when compared to the same measurement conducted at laboratory as the conductor of the coaxial cable in the bus was completely enclosed by the shield. It was also noted that the capacitive coupling measurement from the bus was higher when compared to the lab results due to the effect of capacitors and bleeder resistors. Similar conclusion were also done for twinaxial cable.

5.2 Future work

The future work would be to model the entire cable in 3D with a braided shield. This would provide a better insight on the shielding effectiveness and also analyze the mutual inductance between the cable and shield. A FEM model with a braided shield would also help to analyze the cable impedance depending on its placement for the chassis. The amount of electric and magnetic fields linking the chassis and nearby components could be studied more accurately. The lab measurements has to be improved by including connectors such that the shield completely encloses the conductor. The grounding of cable shields has to be investigated further at higher frequencies.

Bibliography

[1] Henry W. Ott, *Electromagnetic Compatibility Engineering*, Hoboken, New Jersey: John Wiley & Sons, Inc., 2009. [Online]. Available: http://s1.downloadmienphi.net/file/downloadfile5/192/1388769.pdf. Accessed: Feb 14, 2017

[2] S. Alexandersson, "Automotive Electromagnetic Compatibility," Ph.D. dissertation/Lic. thesis, Department of Industrial Electrical Engineering and Automation, Lund University, Lund, Sweden, 2008

[3] Sophocles J. Orfanidis, *Electromagnetic Waves and Antennas*, Piscataway, New Jersey: ECE Department, Rutgers University 2016. [Online]. Available:http://www.ece.rutgers.edu/~orfanidi/ewa/. Accessed: Feb 14, 2017

[4] Several authors. (2014). *System Perspectives on Electromobility*. (2.1) [Online]. Available: http://www.chalmers.se/en/areas-of-advance/energy/Documents/Systems%20Perspectives%20on/Systems_Perspectives_on_Electromobility_2014_v2.1.pdf

[5] Mathias Enohnyaket. (2008, December). State of the Art Report on EMC characterization of hybrid vehicles. EISLAB, Luleå Universitet. Luleå, Sweden. [Online]. Available:https://www.diva-portal.org/smash/get/diva2:998401/FULLTEXT01.pdf

[6] N. Mohan, T. M. Undeland and W. P. Robbins, *Power Electronics Converters, Applications, and Design*, 2nd ed., New York: John Wiley & Sons, Inc., 1995,pp. 500-502.

[7] Kaushik Rajashekara. (2013, March). Present Status and Future Trends in Electric Vehicle Propulsion Technologies. *IEEE Journal of Emerging and Selected Topics in Power Electronics* [Online]. 1 (1), pp. 3-10. Available: http://ieeexplore.ieee.org.proxy.lib.chalmers.se/stamp/stamp.jsp?arnumber=6507304

[8] C. Lugnberg, D. Wenander, Current ripple simulation in DC traction voltage system of an electric bus, Lund Institute of Technology. January, 2017.

[9] Matt McGeehan CA, "Electric vehicles and the sustainability balance sheet," ICAS, 2017. [Online]. Available: https://www.icas.com/technical-resources/are-electric-vehicles-really-more-sustainable. Accessed: July 2017.

[10] William H. Hayt, *Engineering Electromagnetics, Sixth Edition*, New York: The McGraw-Hill Companies, Inc., 1221. [Online]. Available: http://bookzz.org/book/601318/cbed4e. Accessed: Feb 14, 2017

[11] Arthur T. Bradley, Brian J. Yavoich, Shane M. Hodson and Richard F. Godley, "Comparison of Analysis, Simulation, and Measurement of Wire-to-Wire Crosstalk, Part 1", NASA Langley Research Center

[12] Automotive Products, Pfäffikon,Switzerland:Huber+Suhner,2017. [Online]. Available: https://literature.hubersuhner.com/Marketsegments/Transportation/AutoProductCatalogueEN/. Accessed: June 6, 2017.

[13] E.Bogatin, Signal and power integrity. 2th ed., Boston, USA, 2010, pp. 242-243. [Online]. Available: http://www.oldfriend.url.tw/article/SI_PI_book/Signal%20and%20Power%20Integrity%20-%20Simplified_2nd_Eric%20Bogatin_Prentice%20Hall%20PTR_2010.pdf. Accessed: June 8, 2017.

[14] Bode 100 User Manual, Klaus, Austria: OMICRON electronics GmbH, 2017. [Online]. Available: https://www.omicron-lab.com/fileadmin/assets/manuals/Bode-100-User-Manual-ENU10060501.pdf

[15] Elya B. Joffe; Kai-Sang Lock, "Grounding in Wiring Circuits and Cable Shields," in Grounds for Grounding:A Circuit to System Handbook, Wiley-IEEE Press, Country: USA, 2010, ch. 7, pp. 469 - 587. [Online]. Available: http://ieeexplore.ieee.org/xpl/ebooks/bookPdfWithBanner.jsp?fileName=5487804.pdf&bkn=5452231&pdfType=chapter. Accessed:June 8, 2017

[16] Measuring Ultra Low Impedances and PDNs, Klaus, Austria: Steve Sandler and Charles Hymowitz, 2012. [Online]. Available: http://www.picotest.com.tw/Download_File/INJ_um/Application%20Article/Measuring%20Ultra%20Low%20Impedances%20and%20PDNs.pdf